



HAL
open science

S100A8-mediated metabolic adaptation controls HIV-1 persistence in macrophages in vivo

Fernando Real, Aiwei Zhu, Boxin Huang, Ania Belmellat, Alexis Sennepin, Thomas Vogl, Céline Ransy, Marc Revol, Riccardo Arrigucci, Anne Lombès, et al.

► To cite this version:

Fernando Real, Aiwei Zhu, Boxin Huang, Ania Belmellat, Alexis Sennepin, et al.. S100A8-mediated metabolic adaptation controls HIV-1 persistence in macrophages in vivo. *Nature Communications*, 2022, 10.1038/s41467-022-33401-x . hal-03808067

HAL Id: hal-03808067

<https://hal.science/hal-03808067>

Submitted on 10 Oct 2022

HAL is a multi-disciplinary open access archive for the deposit and dissemination of scientific research documents, whether they are published or not. The documents may come from teaching and research institutions in France or abroad, or from public or private research centers.

L'archive ouverte pluridisciplinaire **HAL**, est destinée au dépôt et à la diffusion de documents scientifiques de niveau recherche, publiés ou non, émanant des établissements d'enseignement et de recherche français ou étrangers, des laboratoires publics ou privés.

1 **Peer Review Information:** *Nature Communications* thanks Shokrollah Elahi, Neeltje Kootstra, and the other,
2 anonymous, reviewer(s) for their contribution to the peer review of this work.

3

4

5

6

7

8

9

10

11

12

13

14

15

16

17

18

19

20

21

22

23

24

25

26

27

28

29

30

31

32

33

34

35 **Title**

36 **S100A8-mediated metabolic adaptation controls HIV-1 persistence in macrophages *in vivo***

37

38 **Author list**

39 Fernando Real^{1,2,3}, Aiwei Zhu^{1,2,3}, Boxin Huang^{1,2,3}, Ania Belmellat^{1,2,3}, Alexis Sennepin^{1,2,3}, Thomas Vogl⁴, Céline
40 Ransy^{2,3}, Marc Revol⁵, Riccardo Arrigucci⁶, Anne Lombès^{2,3}, Johannes Roth⁴, Maria Laura Gennaro⁶, Frédéric
41 Bouillaud^{2,3}, Sarra Cristofari⁵, Morgane Bomsel^{1,2,3*}

42

43 **Affiliations**

44 ¹Laboratory of Mucosal Entry of HIV and Mucosal Immunity, Institut Cochin, Université Paris Cité, 75014
45 Paris, France.

46 ²CNRS, UMR8104, 75014 Paris, France.

47 ³Inserm, U1016, Institut Cochin, 75014 Paris, France.

48 ⁴Institute of Immunology and Interdisciplinary Center for Clinical Research, University of Münster,
49 Münster, Germany.

50 ⁵Plastic, Reconstructive and Aesthetic Surgery Department, Saint Louis Hospital, Paris, France.

51 ⁶Public Health Research Institute, New Jersey Medical School, Rutgers, The State University of New Jersey,
52 Newark, New Jersey, USA

53

54 *Corresponding author: morgane.bomsel@inserm.fr

55 Laboratory of Mucosal Entry of HIV and Mucosal Immunity, 3I Department, Cochin Institute, 75014 Paris,
56 France

57 Telephone: +33-1-40-51-64-97

58 Fax: +33-1-40-51-64-54

59

60

61 **Keywords:** HIV-1, mucosa, tissue macrophage, S100A8, M4-macrophages, reservoir, glycolysis

62

63

64

65

66

67

68

69 **Abstract**

70

71 HIV-1 eradication is hindered by viral persistence in cell reservoirs, established not only in
72 circulatory CD4⁺T-cells but also in tissue-resident macrophages. The nature of macrophage reservoirs and
73 mechanisms of persistence despite combined anti-retroviral therapy (cART) remain unclear. Using genital
74 mucosa from cART-suppressed HIV-1-infected individuals, we evaluated the implication of macrophage
75 immunometabolic pathways in HIV-1 persistence. We demonstrate that *ex-vivo*, macrophage tissue
76 reservoirs contain transcriptionally active HIV-1 and viral particles accumulated in virus-containing
77 compartments, and harbor an inflammatory IL-1R⁺S100A8⁺MMP7⁺M4-phenotype prone to glycolysis.
78 Reactivation of infectious virus production and release from these reservoirs *in-vitro* are induced by the
79 alarmin S100A8, an endogenous factor produced by M4-macrophages and implicated in “sterile”
80 inflammation. This process metabolically depends on glycolysis. Altogether, inflammatory M4-
81 macrophages form a major tissue reservoir of replication-competent HIV-1, which reactivate viral
82 production upon autocrine/paracrine S100A8-mediated glycolytic stimulation. This HIV-1 persistence
83 pathway needs to be targeted in future HIV eradication strategies.

84

85 **Introduction**

86

87 Current HIV-1 combination antiretroviral therapy (cART) is neither curative nor eradicates
88 infection largely due to the establishment of cell reservoirs for the virus, which persistently shelter HIV-1
89 through poorly understood mechanisms. Apart from classically described CD4⁺ T-cell reservoirs, HIV-1
90 also establishes and persists in tissue macrophages^{1,2} by integrating viral genome³ into macrophage DNA.
91 Viral genome integration promotes viral replication for weeks post-infection with limited viral lytic egress^{3,}
92 ^{4,5}, and finally resulting in latent macrophage infection⁶.

93 The latency of macrophage infection, i.e. the reversibly nonproductive state of infection⁷ in the
94 weeks following infection has been demonstrated *in vitro* by restoring viral production of infected
95 macrophage after activation of Toll-like receptor 4 (TLR4), the lipopolysaccharide (LPS) receptor⁸ by LPS.
96 Accordingly, LPS is known to reactivate, once silent, integrated proviral DNA^{9, 10, 11}. In chronically or
97 latently infected macrophages, TLR4 engagement induces a signal transduction pathway that culminates in
98 the activation of the nuclear factor-kappa B (NF-κB)¹¹, which in turn efficiently triggers HIV-1 long-
99 terminal repeat (LTR) promoters and HIV-1 replication¹⁰.

100 There is growing evidence that macrophages are directly involved in the persistence of HIV-1 in
101 tissues.^{12, 13, 14}, remaining transcriptionally active HIV-1 despite cART⁷. Similar to tissue-like macrophages
102 infected *in vitro*⁶, infected macrophages detected *in vivo* exhibit pathogen-containing vacuoles also known
103 as virus-containing compartments (VCC). This structure is absent from infected CD4⁺ T-cells that are
104 unable to store viral particles. In macrophages, VCCs might serve as storage compartments for infectious
105 virus produced despite cART and prone to be transferred to other target cells upon external stimulation

106 during cART¹⁵ and/or once antiretroviral therapy is withdrawn¹⁶. We have previously shown that tissue-
107 resident macrophages might constitute an important replication-competent HIV-1 reservoir¹². This
108 macrophage reservoir most likely forms during early tissue-macrophage infection during HIV-1 sexual
109 transmission^{6, 17}. *In vivo*, the degree of plasticity of macrophages is much higher than *in vitro*. Hence, the
110 two main polarization states in which macrophage can be differentiated *in vitro* are the pro-inflammatory
111 M1 and the pro-reparative M2 macrophage subtypes. In contrast *in vivo*, CD68⁺ macrophages from HIV-1-
112 infected cART-suppressed individuals harbor mainly a mixed M1/M2 phenotype expressing the IL-1 and
113 IL-4 receptors, and CD206 but not the M2 marker CD163. As HIV chronic infection is associated to low-
114 level chronic inflammation in the circulation but also in mucosal tissue, such mixed M1/M2 phenotype
115 could correspond to the recently described inflammatory M4-macrophage subtype that contributes to
116 atherosclerosis. This M4-macrophage subtype is characterized by expression of CD68, CD206, the
117 metalloproteinase 7 (MMP7) and the calcium-binding protein A8 (S100A8) and which polarization is
118 dependent on CXCL4/PF4^{18 19 20 21}. However, the precise characteristics of macrophage reservoirs at the
119 single cell level, their capacity to remain transcriptionally active despite cART, and the mechanism
120 supporting persistence of HIV-1 remain elusive.

121 HIV persistence mechanisms profoundly differ between T-cells and macrophages. In the later, it is
122 tightly related to innate immunity inflammatory stimuli²². Furthermore, macrophages are key players in
123 tissue homeostasis and reactive to metabolic adaptations potentially implicated in HIV-1 persistence^{23, 24, 25}.
124 We thus investigated whether mucosal macrophage HIV-1 reservoirs express inflammatory factors
125 controlling reservoir maintenance, and whether in these reservoirs, macrophage metabolism could rule HIV-
126 1 dynamics.

127 Here, we reveal that a specific macrophage subset, the inflammatory M4 one, is prone to glycolysis
128 and constitute the principal viral mucosal reservoir. When facing an inflammatory stimulus such as that
129 induced by the inflammatory alarmin S100 calcium binding protein A8 (S100A8) expressed in particular by
130 tissue M4-macrophages and which can target TLR-4, the M4-macrophage metabolic profile shifts towards
131 glycolysis. Furthermore, S100A8 maintains M4-macrophage reservoir persistence in an autocrine/paracrine
132 loop and reactivates the production of replication-competent viral particles in male genital tract
133 macrophages obtained from cART-suppressed individuals in a process controlled by a glycolytic
134 metabolism adaptation.

135 The characterization of inflammatory M4-macrophages as the major HIV-1 reservoir in the genital
136 mucosa from cART-suppressed individuals, together with the demonstration that macrophage glycolytic
137 immuno-metabolism participates in HIV-1 latency reversal by controlling the production of infectious HIV-
138 1 from these reservoirs, contribute to define novel pharmacological targets for a functional HIV-1 cure.

139

140 **Results**

141

142 **Inflammatory macrophages with an M4 (S100A8⁺MMP-7⁺) phenotype are enriched in the genital**
143 **mucosa of cART-suppressed HIV-1 infected-individuals**

144

145 We previously identified the TLR-4 ligand LPS as an agent capable of reactivating replication
146 competent HIV-1 from genital tissue suspension. This indicated that tissue macrophages might form major
147 replication-competent HIV-1 reservoirs in these mucosa^{6,12}, although the precise identity of these reservoirs
148 remained unclear. We have assessed mucosal macrophages from urethral tissue from healthy and HIV-
149 infected cART-treated individuals (Table 1) by a series of experiments using various techniques as
150 summarized in Figure 1a. First, to determine the distinctive phenotype of HIV-1 reservoirs formed in tissue-
151 resident macrophages at the single-cell level, we profiled the cytokines implicated in the polarization of
152 different macrophage subtypes^{26, 27} in urethral tissue lysate samples from healthy donors and cART-
153 suppressed HIV-1 infected individuals comparatively, using the Luminex technology. C-X-C motif
154 chemokine 4/ Platelet Factor 4 (CXCL4/PF4), Interleukin-13 (IL-13), Interferon- γ and Granulocyte-
155 macrophage colony-stimulating factor (GM-CSF) were upregulated in mucosal tissue from cART-
156 suppressed HIV-infected individuals as compared with non-infected donors (Figure 1b and Supplementary
157 Figure 1a). CXCL4/PF4 directly correlated with IL-13 independently of the HIV status. However, only in
158 the cART HIV⁺ group, CXCL4/PF4 correlated directly with IFN- γ and inversely with IL-4 (Supplementary
159 Figure 1b). The upregulation of CXCL4/PF4 in cART-suppressed HIV-infected individuals compared with
160 healthy donors was confirmed by immunohistochemistry (Supplementary Figure 2).

161 IL-13 is implicated in the alternative activation of macrophages resulting in a pro-reparative
162 CD206⁺CD163⁺ macrophage subset that antagonizes IFN- γ inflammatory actions and is implicated in
163 humoral immunity, allergies and anti-parasitic responses²⁸. The participation of *bona fide* pro-reparative
164 CD163⁺ macrophages to HIV-1 tissue reservoirs could be discarded based on our recent results showing that
165 CD163^{neg} but CD206⁺IL4-R⁺IL1-R⁺ macrophages with an intermediate pro-inflammatory/pro-reparative
166 profile are enriched in urethral tissue of cART-treated patients¹², and are the likely site of HIV persistence
167 in the male genital mucosa. However, IL-13 can also drive macrophage expression of DC-SIGN, an
168 alternative receptor for HIV-1, thus rendering macrophages highly susceptible to HIV infection. The
169 upregulation of IL-13 in mucosal tissues from cART-suppressed HIV-1-infected patients we observed might
170 result from the immunomodulatory activity of CXCL4/PF4 on Th2 lymphocytes²⁹.

171 Furthermore, CXCL4/PF4 is mainly expressed by cells of the megakaryocyte lineage and
172 consequently in platelets but also by some epithelial cells^{26, 30}. One function of CXCL4/PF4 is to induce *in*
173 *vitro* the polarization of macrophages toward the recently described M4 subset³¹, an inflammatory
174 macrophage subset related to foam cell formation, atherosclerosis and intracellular infection^{26, 30}. M4-
175 macrophages express inflammatory surface markers such as HLA-DR and CD86 but lack CD163²⁶. Such
176 macrophage profile matches that of CD163^{neg} but CD206⁺IL4-R⁺IL1-R⁺ activated macrophage subtype we
177 have found implicated in mucosal persistence of HIV-1¹². M4-macrophages are defined, both *in vitro* and *in*
178 *vivo*, by the co-expression of the S100 calcium binding proteins (S100) A8 and S100A9 also known as

179 Myeloid-related protein 8 and 14 (MRP8 and MRP14) or Calgranulin A^{30, 32}, along with metalloproteinase
180 7 (MMP-7)³³. The markers CD68⁺S100A8⁺MMP-7⁺ thus identify M4-macrophages.

181 To search for M4-macrophage in urethral tissues in HIV/AIDS, we analyzed the frequency of total
182 mucosal (CD68⁺) macrophages in urethral cell suspensions and therein, the frequency of M4-macrophages
183 (S100A8⁺MMP-7⁺) by flow cytometry (Figure 1c-d and Supplementary Figure 3). Although the frequency
184 of macrophages did not differ between healthy donors and cART-suppressed HIV-infected individuals, M4-
185 macrophages were enriched in urethral tissues from the HIV-1 infected group compared with healthy donors
186 (Figure 1c-d). The expression of common markers of macrophage polarization in total urethral macrophages
187 (CD68⁺) as well as in M4-macrophages was also investigated. We observed an increased frequency of
188 macrophages expressing the inflammatory markers CD86 and IL-1R among both total macrophages (Figure
189 1e left for frequencies and Supplementary Figure 3d left for MFI) and M4-macrophages (Figure 1e right for
190 frequencies and Supplementary Figure 3d right for MFI) from cART-suppressed HIV-1 infected individuals
191 compared with healthy donors.

192

193 **Inflammatory IL-1R⁺ M4-macrophages are the main HIV-1 mucosal macrophage reservoirs *in vivo***

194

195 The macrophage HIV reservoirs found in the urethral mucosal stroma from cART-suppressed
196 individuals are a transcriptionally active reservoir in which HIV RNA was detected by fluorescent *in situ*
197 hybridization (FISH) (Figure 2a). We quantified HIV-1-infected macrophages in urethral tissues from
198 cART-suppressed individuals at the single-cell level combining FISH and flow cytometry referred to as
199 FISH-flow^{34, 35} to detect cell-associated HIV together with markers of different macrophage profiles,
200 including the M4-defining S100A8 and MMP-7. We first validated the FISH-flow HIV-1 RNA probes using
201 OM-10.1 cell lines (Supplementary Figure 4a-b) which constitutively harbor integrated HIV provirus and
202 can be stimulated to produce more HIV-1 upon TNF- α stimulation³⁶.

203 In HIV-1-infected individuals despite cART-suppression, we detected a subpopulation of
204 macrophages containing HIV-1 RNA and the viral capsid protein p24 (Gag) that represents 0.3% [CI: 0.12-
205 0.48] of total mucosal macrophages present in tissue cell suspensions (Figure 2b-c and Supplementary
206 Figure 4c).

207 To characterize these HIV⁺ macrophages, we generated UMAPs from the multiparametric flow
208 cytometry analysis including S100A8, MMP-7, IL-1R, IL-4R, CD206 and CD163 markers and compiling
209 data from 4 cART HIV⁺ individuals. The rare HIV⁺ macrophages detected were backgated into this UMAP
210 (Figure 2d). The results showed that HIV⁺ macrophages were distributed in the M4 population (light blue
211 population in UMAP, S100A8⁺MMP-7⁺CD206⁺IL-1R⁺) and in a second population (purple population in
212 UMAP) characterized by S100A8^{neg}MMP-7⁺CD206⁺IL-1R⁺ macrophages. Around half of the infected
213 macrophages (52.7 % [CI: 16.6-100]) belonged to the S100A8⁺MMP-7⁺ M4-macrophage profile
214 (Supplementary Figure 4d). Furthermore, these HIV-1-infected macrophages expressed also CD206, IL-4R
215 and IL-1R but not CD163 (Figure 2d and Supplementary Figure 3d), in agreement with the previously

216 uncharacterized CD206⁺IL4-R⁺IL1-R⁺CD163^{neg} intermediary subset (Mi) of macrophages we found
217 enriched in the male urethra of cART-suppressed individuals¹². Finally, S100A8 was expressed by the
218 macrophage HIV reservoirs as demonstrated by the immunodetection of S100A8 within HIV-1 reservoirs
219 identified as CD68⁺/HIV-1 RNA⁺ cells using combined immunohistochemistry and RNAscope FISH
220 (Figure 2e).

221 Altogether, we have identified a transcriptionally active (HIV-1 RNA⁺) reservoir formed mainly in
222 M4-macrophages that express the pro-inflammatory activation marker IL-1R and, importantly, the alarmin
223 S100A8.

224

225 ***In vitro* derived and latently infected M4-macrophages are surrogates of HIV-1 mucosal macrophage** 226 **reservoirs**

227

228 As mucosal tissues from HIV-1 infected individuals are rare, hampering the characterization of HIV
229 reservoir dynamic, we established alternative models of HIV-1 reservoir in macrophages, either from
230 monocytes or from tissue macrophages infected *in vitro* until latency self-establishment.

231 M4-macrophages can be differentiated from blood monocytes *in vitro* by culture in the presence of
232 CXCL4/PF4^{30,32}, resulting in M4-monocytes derived macrophages (MDM). We first investigated whether
233 M4-MDM would be surrogates of the tissue macrophages found in the urethral mucosa by flow cytometry.
234 Relative to the expression of tested macrophage surface markers, especially S100A8, one subunit of the
235 heterodimeric S100A8/S100A9 complex, we found that M4-MDM were more closely related to the
236 population of urethral macrophages isolated either from HIV-1-infected or healthy individuals than other *in*
237 *vitro* derived macrophage subtypes, namely “classically” activated pro-inflammatory M1-MDM (induced by
238 GM-CSF, IFN- γ and LPS) and alternatively activated pro-reparative M2-MDM (induced by M-CSF, IL-4
239 and IL-13) (Figure 3a).

240 When infected with HIV-1, the different MDM subsets were productively infected. At later time
241 points, whereas non-polarized-MDM induced by GM-CSF/M-CSF or M2-MDM, although at a lower level
242 in agreement with others^{3,24}, continue both to produce viral particles until day 49 after infection as detected
243 by p24 ELISA, M4-MDM reduced viral production and enters latency characterized by undetectable viral
244 production from day 8.5 [CI: 7-15] (Figure 3b).

245 At the morphological level, M4-MDM harbored viruses in virus-containing compartments (VCCs)
246 (Figure 3c) during the latent phase of viral production, i.e., when macrophages stop producing new viral
247 particles into the culture medium. Similarly, in mucosal tissues CD68⁺ macrophages sheltered HIV-1 in
248 VCCs as detected by p24 labeling (Figure 3d). We next performed morphometric analyses of VCCs formed
249 *in vitro* by latently infected M4-MDM (Figure 3e) and formed *in vivo* by mucosal macrophages in tissues
250 (Figure 3f). These analyses revealed that although VCCs in M4-MDM were more heterogeneous in size,
251 number and scattering, the sum of the VCCs volume per infected macrophage did not differ from that in

252 infected mucosal tissue macrophage reservoirs formed *in vivo*. A panel of additional macrophage VCCs
253 detected *in vivo* in tissues is shown in Supplementary Figure 5a.

254 Finally, we also infected genuine mucosal tissue macrophages purified from healthy donor tissue by
255 HIV-1 *in vitro*. Tissue macrophages were productively infected by HIV-1 in a similar manner to M4-MDM,
256 but established latency even earlier, reaching latency after a median interval of 5 [CI: 3-10] days post-
257 infection (Figure 3g) compared with 8.5 [CI: 7-15] days post-infection for M4-MDM. Viral production by
258 *ex vivo*-infected urethral macrophages is abrogated by the antiretroviral drug Zidovudine (AZT), confirming
259 productive infection (Figure 3h).

260 We thus established two reliable surrogates of the tissue macrophage reservoirs found in urethral
261 mucosa, formed by M4-MDM and tissue macrophages acutely infected *in vitro* by HIV-1 and maintained at
262 least for a week in culture.

263

264 **S100A8 can reactivate the production of replication-competent virus from macrophage reservoirs**

265

266 S100A8 is always expressed together with S100A9 as a heterodimer³⁷. However, to show the full
267 activity of the S100A8/S100A9 complex, it is necessary to use S100A8 homodimers in cell culture studies
268 because the activity of the heterodimer is very low *in vitro* due to the formation of heterotetramers that
269 blocks the S100A8/S100A9 complex activity³⁷.

270 S100A8/S100A9 activates specifically TLR4³⁸, which in turn can reactivate HIV-1 production³⁹.
271 We thus hypothesized that formation and persistence of HIV-1 reservoirs in M4-macrophages is regulated
272 by a local S100A8/S100A9-mediated low-level HIV-1 production in genital tissues. When secreted in
273 tissues, mainly from neutrophils or macrophages, S100A8/S100A9 forms rapidly heterotetramers³⁷, thereby
274 buffering its activity. It might remain nevertheless a short window of time during which the
275 S100A8/S100A9 heterodimer could be active locally in an autocrine/paracrine fashion.

276 We thus measured the levels of S100A8 monomer and S100A8/S100A9 heterodimers in urethral
277 tissues by ELISA. S100A8/S100A9 heterodimer, the physiologically relevant form, was expressed at much
278 higher concentration than the S100A8 monomer, as expected. Furthermore, the S100A8/S100A9
279 heterodimer concentration was significantly reduced in cART-suppressed HIV-1-infected individual as
280 compared with healthy donor tissues (Figure 4a), in line with increased neutrophil cell death observed in
281 HIV-infected individuals on cART⁴⁰.

282 We further investigated whether the measured tissue S100A8 and its expression at the tissue
283 macrophage level were associated. When analyzed by flow cytometry, the frequency of S100A8⁺ cells
284 remained similar in both healthy donors and HIV-1-infected individuals. However, the expression of
285 S100A8 per cell, corresponding to the MFI, was specifically upregulated in M4-macrophages isolated from
286 cART-suppressed HIV-1-infected individuals compared with tissue M4-macrophages from non-infected
287 individuals but also with cells from the entire tissue cell population and total tissue macrophage population
288 of infected and non-infected individuals (Figure 4b). Therefore, although the total mucosal tissue

289 S100A8/S100A9 heterodimer level was decreased in cART-suppressed infected individuals, the level of
290 S100A8 was higher in M4-macrophages from cART-suppressed infected individuals, the main macrophage
291 subset that host HIV-1, compared with healthy donor ones. In tissue from cART- treated individuals that are
292 subjected to chronic low-level inflammation ⁴¹, S100A8 could be locally secreted upon M4-macrophage
293 stimulation and act in an autocrine/paracrine manner to reactivate the macrophage reservoirs upon binding
294 to TLR4.

295 To investigate the capacity of S100A8 to reverse HIV-1 latency in macrophage reservoirs, we first
296 evaluated whether S100A8 treatment would reverse latency in HIV-1-infected M4-MDM. For these cell
297 culture-based studies, we used the homodimer S100A8 instead of the physiological relevant heterocomplex
298 S100A8/S100A9 due to the rapid loss of activity by heterotetramerization ³⁷. S100A8 resumed viral
299 production from a HIV-1 latent state in M4-MDM (Figure 4c) in a concentration-dependent manner from 5
300 to 20µg/ml, as measured by p24 ELISA. Latency reversal by S100A8 was as efficient as that induced by
301 LPS at a concentration of 1 µg/ml, a treatment we and others have already shown to reactivate HIV-1
302 production from macrophages latently infected by HIV *in vitro* or *in vivo* ^{6,12}. Moreover, in latently infected
303 M4-MDM, HIV DNA was found integrated in the host cell genome, as measured by Alu-gag nested PCR
304 (Supplementary Figure 5b, left). Addition of S100A8 to latently infected M4-macrophages resumed viral
305 transcription. S100A8-mediated viral reactivation is specific, as the antiretroviral drug AZT blocked it to
306 level prior to reactivation (Supplementary Figure 5b, right).

307 Furthermore, S100A8 at 10µg/ml was also efficient at reactivating viral production from mucosal
308 tissue macrophages isolated from healthy donors and latently infected by HIV-1 *in vitro* used as another
309 HIV-1 macrophage reservoir surrogate (Figure 4d).

310 Finally, S100A8 reversed latency in tissue macrophages isolated from cART-suppressed HIV-1-
311 infected individuals. The reactivated virus was replication-competent as quantified in a viral outgrowth
312 assay using activated CD4⁺ T-cells (Figure 4e). Additionally in tissues from cART-treated individuals, HIV-
313 1 RNA *in situ* hybridization coupled to p24-Gag immunodetection in CD68⁺ macrophages further
314 demonstrated that clusters of p24 (Gag) proteins co-localized with HIV-1 RNA, a pattern suggestive of
315 VCCs before *ex vivo* S100A8 treatment (Supplementary Figure 5c upper). Upon S100A8-mediated HIV-1
316 reactivation, both HIV-1 RNA and protein relocalized at the macrophage plasma membrane that is
317 suggestive of extemporaneous production of new HIV-1 particles and/or mobilization of VCCs to the
318 macrophage plasma membrane in the process of releasing their virus content (Supplementary Figure 5c
319 lower).

320

321 **S100A8-mediated reactivation of HIV-1 release from macrophage reservoirs depends on glycolysis**

322

323 After engaging TLR4, microbial components such as LPS trigger a pro-inflammatory response in
324 macrophages that was recently described to engage a metabolic reprogramming, which contributes to
325 macrophage plasticity and physiology ⁴². As we have shown that mucosal macrophage HIV-1 reservoirs

326 express pro-inflammatory markers (Figures 1 and 2), we investigated whether S100A8-mediated
327 reactivation of the mucosal macrophage reservoirs would trigger a similar metabolic reprogramming related
328 to inflammatory responses.

329 The macrophage metabolic profile varies according to macrophage polarization from pro-reparative
330 to pro-inflammatory macrophages. In “classically” IFN- γ /LPS activated M1-macrophages, aerobic
331 glycolysis is induced, as well as a glucose-induced repression of respiration, beneficial for aerobic
332 glycolysis what is known as the Warburg effect in cancer cells⁴³. “Alternative” IL-4/IL-13-activated M2-
333 macrophages obtain energy preferentially from fatty acid oxidation and oxidative metabolism via oxidative
334 phosphorylation (OXPHOS)⁴². Little is known about the metabolism of other alternative macrophage
335 subsets implicated in inflammatory diseases such as the M4 subset⁴⁴. We thus first investigated the
336 metabolic profile of *in vitro*-derived inflammatory M4-macrophages compared with pro-reparative M2-
337 macrophages. Therefore, M2- and M4-MDM basal metabolism was evaluated comparatively by measuring
338 extracellular acidification rate (ECAR, to assess glycolysis) and oxygen consumption rate (OCR, to assess
339 OXPHOS) upon injection of glucose into macrophage cultures. As a result, M4-MDM presented a mixed
340 metabolic profile, carrying out glycolysis (inhibited by 2-deoxyglucose, or 2-DG) but also fatty acid
341 oxidation (inhibited by etomoxir). Upon glucose addition to culture medium, M4-MDM glycolytic activity
342 was higher than that of M2-MDM (Figure 5a left) whereas M4-MDM OCR was only slightly repressed
343 compared to that of M2-MDM (Figure 5a right). By adding metabolic inhibitors to macrophages during
344 their metabolic evaluation, the glycolytic activity of these cells could be recorded. As a result, M4-
345 macrophages had a higher glycolytic activity than M2 macrophages (Figure 5b). As compared with M2-
346 MDM which glycolytic activity remains close that of baseline after glucose addition, M4 were more prone
347 for glycolysis. Indeed, after addition of glucose, M4-MDM glycolysis activity increased by 25% from
348 baseline (Supplementary Figure 6a). These data define M4-macrophages as a pro-inflammatory, glycolytic
349 subset among the spectrum of different macrophage immunometabolic profile.

350 Next, we evaluated the metabolic responses of M4-macrophages in glucose-supplemented medium
351 after injection of medium alone (untreated), S100A8 (that we have shown above to act as HIV-1 latency
352 reversal agent) or LPS. S100A8 triggered a significant glycolytic activity of M4-MDM, higher than that in
353 the absence of stimulation, but less intense than the LPS-stimulated glycolysis (Figure 5c left and Fig. 5d).
354 We observed an increase in glycolysis activity of ~15%, ~40% and ~60% from baseline after injection of
355 medium alone (untreated), S100A8 and LPS, respectively (Supplementary Figure 6b).

356 In contrast, S100A8 did not affect the OCR whereas LPS slightly decreased it (Figure 5c right)
357 Altogether, LPS and S100A8 affected M4-macrophages metabolism by increasing mainly glycolysis with
358 no major impact on cell mitochondrial respiration. These differences in the intensity of glycolytic activity in
359 M4-macrophage upon stimulation by S100A8 and LPS may explain the difference in the intensity of latency
360 reversal observed in M4-macrophage reservoirs treated with these two compounds

361 We next evaluated whether latency reversal in HIV-1 macrophage reservoirs can be triggered upon
362 glycolytic stimulation via TLR4. Therefore, *in vivo* established tissue macrophage reservoirs obtained from

363 cART-suppressed HIV-1-infected individuals were treated with S100A8 to resume the production of
364 replication-competent HIV-1 in the absence of or with pretreatment with the glycolytic inhibitor 2-DG as
365 schematized in Figure 5e. S100A8 triggered HIV latency reversal in tissue macrophage reservoirs resulting
366 in infectious virus production in the culture medium, as quantified in the outgrowth assays using CD4⁺T-
367 cells as reporter cells (Figure 5f). Inhibition of glycolysis before induction of latency reversal by S100A8
368 fully blocked the reactivation of replication-competent viral production by macrophages (Figure 5f).
369 Altogether, immunometabolic glycolytic pathways control HIV-1 reservoir reactivation in tissue
370 macrophages.

371

372 **Discussion**

373

374 The characterization of the degree of differentiation/polarization toward a specific macrophage
375 subtype capable of hosting HIV-1 in human mucosal tissues permits to identify a central host cell
376 therapeutic target for the virus in male genital mucosa. Macrophages are known to be extremely versatile
377 cells, able to respond to a plethora of factors by differentiating into functionally distinct subsets. Each
378 issue-specific environment, presenting a characteristic set of cytokines, could drive macrophages towards a
379 HIV-1-resistant or -susceptible state, not necessarily associated to the *in vitro* established M1/M2
380 macrophage polarization paradigm^{3, 27}. Our study is the first, to our knowledge, to measure macrophage-
381 related cytokines in the urethral mucosa comparing healthy donors and HIV-infected individuals under
382 cART. Despite effective blood viral suppression by cART, HIV-infected individuals present persistent
383 chronic immune activation, albeit at low levels in blood and tissues^{41, 45, 46}. Resulting change in
384 microenvironment could polarize macrophages toward specialized profiles implicated in viral persistence.

385 Here, we demonstrated that in the urethral tissue from cART-suppressed HIV-infected patients, the
386 HIV-1 replication-competent reservoir resides in a recently described subtype of inflammatory macrophages
387 classified as M4. M4 polarization is mainly induced by CXCL4/PF4^{18, 19, 20, 21} that we have found
388 upregulated in the urethral mucosa of cART-suppressed HIV⁺ individuals as compared with healthy donors.
389 Macrophages in most tissues are derived from embryonic progenitors, displaying long life span and self-
390 renewal capacities, and blood monocytes contribute only minimally to the pool of tissue macrophages under
391 homeostatic conditions⁴⁷. However additionally, persistent tissue inflammation as commonly observed in
392 HIV infection⁴⁸ might also contribute to reservoir establishment and persistence. Such persistent tissue
393 inflammation would favor the entry and integration of monocytes in the resident macrophage pool in tissues
394⁴⁷, likely impacting viral reservoirs dynamics. Stable tissue HIV reservoirs would persist long-lived tissue
395 macrophages, likely formed upon their early infection during sexual transmission^{6, 17}. In addition,
396 inflammatory macrophages-derived from blood monocytes⁴⁷ might also either replenish the macrophage
397 reservoir by becoming infected or stimulate the production of viruses sheltered by latently infected
398 macrophages once monocytes enter tissues. Furthermore, such monocyte-derived macrophages repopulating
399 tissues and acquiring self-renewal capacities⁴⁷ could in turn be infected and become HIV reservoirs locally.

400 This could explain how the latently infected pool of macrophages in mucosal tissues is long-lasting and
401 persists despite cART.

402 In this latter context, the production of endogenous inflammatory factors by monocytes such as
403 alarmins can engage TLR and participate in endogenous “sterile” inflammation processes³⁷. This would in
404 turn promote a local tissue autocrine feedback loop favoring low-level of NF-κB-mediated HIV production
405 despite systemic viral suppression. Such scenario is in agreement with the presence of whole viral particles
406 in VCCs that we observed *in vivo* in reservoir macrophages in cART-suppressed patient tissues¹². Unlike T
407 cells, macrophages produce viral particles that mainly bud into and are stored in VCCs¹⁶. VCCs may thus
408 contain incoming as well as *de novo* produced viruses. In the present model, latently infected M4-
409 macrophages containing VCCs stop producing p24 to the extracellular milieu several days p.i., suggesting
410 that the source of virus detected in VCCs is likely not recently endocytosed virus. However, during the
411 phase of active production of virions by infected macrophages, viruses could not only bud into VCCs¹⁶, but
412 could be also endocytosed and stored in VCCs, a feature requiring further investigations for which the M4
413 model is particularly useful.

414 The presence of virus in VCCs we observed further indicates that these infected tissue macrophages
415 form a low-level productive reservoir, as suggested by others⁴⁹. Maintenance of such low-level replication
416 HIV-1 reservoirs, i.e., with sustained low-level viral production despite successful antiretroviral therapy,
417 would involve a perennial inflammatory stimulus such as those observed in non-resolving inflammation, a
418 chronic condition regulated by macrophages^{50,51}.

419 Produced largely by neutrophils and macrophages, S100A8 forms a heterodimer with the S100
420 calcium binding protein A9 (S100A9 or MRP14), and this S100A8/S100A9 complex functions as pro-
421 inflammatory damage-associated molecular patterns (DAMP)^{37,38,52}. S100A8 is however the functional unit
422 of the heterodimer able to engage TLR4³⁸ that in turn activates NF-κB⁵³. This mechanism of action
423 converges with HIV-1 reactivation: indeed, S100A8 activates HIV-1 transcription in latently infected
424 macrophages⁵⁴ and in CD4⁺ T lymphocytes via the NF-κB axis³⁹. Therefore, S100A8 could act as the
425 exogenous bacterial component LPS by activating TLR-4 signaling, although less strongly and without
426 affecting the cell oxygen consumption and mitochondrial respiration. S100A8 might thus be an
427 inflammatory endogenous tissue factor able to stimulate the viral reservoir formed in latently infected
428 macrophages to resume viral production.

429 Of note, S100A8 systemic levels are increased in HIV-1 patients as well as in other inflammatory
430 diseases and viral infections^{38, 54, 55, 56}. Furthermore, S100A8 levels rise also in genital mucosal secretions
431 from HIV-1 infected patients where it can reactivate HIV-1 replication in latently infected cells⁵⁴. However,
432 in the context of antiretroviral therapy, we found that total S100A8 measured as heterodimer with S100A9
433 is down regulated in the urethral mucosa of cART-suppressed HIV-1-infected individuals compared with
434 healthy donors. This decrease could be due to a decrease in the mucosa of cART-treated HIV-infected
435 individuals in the frequency of tissue neutrophils that is the most abundant source of S100A8/S100A9 in
436 tissues³⁸. Therefore, the specific up-regulation of this alarmin in M4-macrophages we observed in cART-

437 suppressed HIV-1-infected individuals compared with healthy donors indicates that S100A8-induced HIV-1
438 reactivation in macrophage reservoirs likely occurs at a local level under mechanisms remaining to be
439 elucidated. One can propose that S100A8, produced locally by M4-macrophages in a short time window
440 prior the formation of heterotetramers with S100A9, binds immediately after secretion and in an
441 autocrine/paracrine manner to TLR-4 at the M4-macrophage reservoir surface. This interaction would
442 secure a regulatory mechanism for controlling the conversion from HIV-1 deep latency observed in CD4⁺ T-
443 cells⁵⁷ toward HIV active transcription and storage of virions in VCCs^{12, 16} that we describe here.

444 One of the mechanisms regulating HIV-1 latency could be a metabolic reprogramming, a process
445 central in macrophage pro-reparative/pro-inflammatory plasticity and in response to pathogens^{58, 59}. Upon
446 pattern recognition receptors (PRR) that engage DAMPs like S100A8 or pathogen-associated molecular
447 patterns (PAMP) like LPS, macrophages rewire their transcriptional program to produce inflammatory
448 factors and metabolic mediators responsible for the modification of macrophage metabolism for aerobic
449 glycolysis, simultaneously⁵⁹. LPS and S100A8 reverse HIV-1 latency in mucosal macrophage reservoirs,
450 both factors inducing an inflammatory reaction and a glycolytic activity. This property could be used for the
451 elimination of HIV-1 reservoirs⁶⁰. Drugs could be developed to target the glycolytic metabolic pathways,
452 offering an alternative, yet unexplored, for shock-and-kill or block-and-lock strategies. The advantage of
453 such an approach is that macrophages can be “trained” upon recognition of inflammatory stimuli, rewiring
454 their metabolism for days or months, as described in other infectious diseases⁶¹. Such long-lasting
455 glycolytic stimulus would keep macrophage reservoirs producing virus until their recognition and
456 elimination by CD8⁺ cytotoxic T lymphocytes (CTL)-mediated killing, to which macrophages are resistant
457 when acutely infected⁶². Pharmacological inhibition of glycolysis is known to profoundly interfere with the
458 physiology of HIV-1 latently infected cells and HIV-1 reactivation^{24, 25}. Therefore, a prolonged shift in
459 glycolytic pathways towards different metabolic profiles could prevent macrophage reservoirs from
460 producing viruses, in turn blocking a potential low-level replication of persistent HIV-1 in tissues.

461 Such blockade of glycolysis could also be exploited to eliminate the HIV-1 reservoir in CD4⁺T-
462 cells. Indeed, a glycolytic environment is required to carry out HIV-1 reverse transcription, and inhibition of
463 glycolysis blocks HIV-1 replication, as recently demonstrated²⁵. Altogether, the metabolism of cells
464 targeted by HIV-1, either CD4⁺T-cells or macrophages, emerges as an important common determinant of
465 HIV-1 infection, even if regulated by different mechanisms.

466 Overall, our results reveal that a specific macrophage subset, the inflammatory M4 one, forms viral
467 mucosal HIV-1 reservoir and promotes viral persistence that is regulated by the endogenously expressed
468 S100A8, which would mediate sustained low-level HIV-1 production in the male genital tract. Such novel
469 HIV-1 reservoir in M4-macrophages adds to the blood T-cell reservoir and now needs also to be targeted by
470 eradication strategies. The requirement for glycolysis in HIV-1 reservoir reactivation reveals a stage of
471 vulnerability that can be exploited in future HIV-1 cure strategies.

472

473 **Methods**

474

475 **Ethical statement.** The study was conducted under local ethical regulation after approval by the local ethical
476 committee (Comité de Protection des Personnes, Île de France XI; approval number 11 016). Human
477 samples were obtained after written informed consent from all study participants.

478

479 **Urethral mucosa tissue cell suspensions and sorting of monocytic/macrophagic urethral cells.** Penile
480 tissues were obtained from individuals undergoing elective gender reassignment surgery at the Saint Louis
481 Hospital in Paris, France. These included healthy individuals and also HIV-infected ones (median age of 43
482 years old [CI: 37-49], infected with HIV-1 for a median duration of 11.5 years [CI: 4-17]) under suppressive
483 cART for a median period of 9.5 years [4-12.9] with undetectable plasma viral loads (<40 RNA copies/ml)
484 for at least 12 months before surgery (Table 1). Immediately following surgery, the penile tissues were
485 preserved in phosphate-buffered saline (PBS) supplemented with 100 U/ml penicillin and 100 µg/ml
486 streptomycin (Gibco, ThermoFisher Scientific) and transported on ice to a biosecurity level 2+ facility.
487 Tissues were processed to obtain a tissue cell suspension of urethral mucosal cells as described¹⁷. Viability
488 of tissue macrophages after tissue processing was evaluated by DRAQ7 staining (BD biosciences) following
489 manufacturer instructions, before and after removal of dead cells by magnetic isolation (dead cell removal
490 kit, Miltenyi Biotec GmbH). Accordingly, viable macrophages corresponded to >90% (before) and >95%
491 (after dead cell removal) of cells among the population of total tissue macrophages (CD68⁺) in the cell
492 suspension (Supplementary Figure 3a).

493 The CD14⁺CD16⁺ cell population was sorted from total tissue cell suspensions using magnetic
494 microbeads (Miltenyi Biotec GmbH) following manufacturer instruction. A mean percentage of 58% [CI:
495 49.12-66.8] cells in the CD14⁺CD16⁺ selected urethral mucosal cell population corresponds to CD68⁺
496 macrophages with less than 1% corresponding to CD3⁺ T-cells, as quantified by flow cytometry. Potential
497 CD3⁺ cell contaminants were thoroughly washed out from the plates before *ex vivo* macrophage cultivation,
498 infection and latency reversal experiments.

499

500 **Ex vivo cultivation of urethral macrophages.** The total CD14⁺CD16⁺ urethral mucosal cell population was
501 cultivated in flat-bottom well plates (5x10³ cells per mm² of well area) to which mainly macrophages
502 remained attached after overnight incubation at 37°C 5% CO₂ and non-adherent or less adherent cells were
503 thoroughly washed out. The remaining attached tissue macrophages were then cultivated in RPMI 1640
504 culture medium supplemented with 10% fetal calf serum (FCS) and employed for *in vitro* HIV infection or
505 HIV latency reversal assays.

506

507 **Monocyte isolation and macrophage culture.** CD14⁺ cells (monocytes) peripheral blood mononuclear cells
508 (PBMCs) obtained by negative selection (STEMCELL Technologies Inc.) according to manufacturer
509 instruction were differentiated *in vitro* into macrophages. Monocyte derived macrophage (MDM) subtypes
510 were obtained using the following regimens in RPMI 1640 with 10% FCS: i) for M1-macrophages: 6 days

511 of 50 ng/ml granulocyte-macrophage colony-stimulating factor (GM-CSF, R&D Systems) followed by 20
512 ng/ml interferon gamma (IFN- γ , R&D Systems) and 1 μ g/ml lipopolysaccharide (LPS from *Salmonella*
513 *enterica* serotype typhimurium, Sigma-Aldrich) for additional 2 days; ii) for M2a-macrophages: 6 days of
514 25 ng/ml macrophage colony-stimulating factor (M-CSF, R&D Systems) followed by 20 ng/ml interleukin 4
515 (IL-4, R&D Systems) and 20 ng/ml IL-13 (R&D Systems) cytokines for additional 2 days⁶³; or 3 iii) for
516 M4-macrophages: 30 μ g/ml C-X-C motif chemokine 4/Platelet Factor 4 cytokine (CXCL4/PF4, Chromatec
517 GmbH) for 6 days^{26, 31}. Non-polarized MDM were produced by cultivation in complete medium
518 supplemented with 50 ng/ml GM-CSF and 25 ng/ml M-CSF for 6 days.

519

520 **In vitro and ex vivo HIV infection.** *In vitro* and *ex vivo* infection experiments were performed using MDM
521 from healthy donors or urethral tissue macrophages respectively, cultivated in the presence of 20 ng/ml
522 [p24-Gag] R5-tropic HIV-1 primary isolate (93BR029, NIH AIDS Reagents program) for 2 hours. Virus
523 was then removed by thorough washes and fresh complete medium was added to macrophage cultures.
524 Zidovudine (AZT) (NIH AIDS Reagent Program) was added at 10 μ M to *ex vivo*-infected tissue
525 macrophages as negative control when quantifying productive infection. Viral production in the days
526 following infection was quantified in culture supernatants by enzyme-linked immunosorbent assays
527 (ELISA) for HIV-1 p24-Gag (p24 Innostest HIV-1 ELISA, InGen, Diaxonhit group, France) for up to 60
528 days. We defined that viral latency was reached when viral detection in the macrophage culture supernatants
529 become undetectable by the p24 ELISA employed as we described⁶. Integrated HIV DNA was assessed by
530 Alu-gag nested PCR as described¹².

531

532 **Latency reversal assays.** Latently infected macrophages, either infected *in vitro* or selected from urethral
533 tissue of cART-suppressed HIV-infected individuals were treated with 1 μ g/ml of bacterial LPS which
534 reactivates viral production^{6, 9, 11, 12}, and with 5 to 20 μ g/ml of purified S100 calcium binding protein A8
535 (S100A8)³⁷. LPS or S100A8 were added to macrophage cultures for 48 hours to reactivate viral production
536 that was then measured in culture supernatants.

537 In latently infected M4-MDM, p24-Gag ELISA was performed directly on culture supernatants after
538 48 hours of latency reversal with LPS or S100A8 (5 to 20 μ g/ml). Cell fractions were processed for HIV-1
539 LTR RT-qPCR as described⁶⁴. Reversal of HIV latency was carried out in the presence of 10 μ M
540 Zidovudine (AZT) in some experiments.

541 In tissue macrophages obtained from healthy donors and latently infected *in vitro*, p24-Gag ELISA
542 was performed in the days following infection until HIV-1 production becomes undetectable by this
543 method. Next, the tissue macrophages were reactivated with LPS or S100A8 (10 μ g/ml) for 48 hours and
544 the macrophages were processed for HIV-1 LTR RT-qPCR as described⁶⁴. To take into account the
545 variability in the acute HIV-1 infection level of tissue macrophages in different donor samples, the amount
546 of virus produced upon reactivation was expressed by the ratio between the number of HIV-1 LTR copies

547 found in reactivated macrophages and the maximal cumulative production of p24-Gag detected by ELISA
548 before the latency.

549 In tissue macrophage reservoirs obtained from cART-suppressed HIV-1-infected individuals and
550 reactivated *ex vivo* with LPS or S100A8 (10 µg/ml), supernatants were collected 48 hours after reactivation.
551 To amplify the small amounts of replication competent virus produced in this case, supernatants were added
552 to CD4⁺ T-cell lymphoblasts in a viral outgrowth assay, as described below.

553

554 **Low-level infectious HIV production assessed by viral outgrowth assays.** Due to the limited amount of
555 latently infected macrophages generated *in vitro*²⁴ or obtained *in vivo*¹² and also as the amount of virus
556 released into culture supernatant from latently infected macrophages reactivated *in vitro* is below the limit of
557 detection for most conventional techniques, it was necessary to amplify the reactivated HIV by an
558 outgrowth assays using CD4⁺ T-cell lymphoblasts^{12, 65}.

559 Accordingly, the production of replication-competent virus following HIV latency reversal of
560 infected macrophages was quantified by an adapted viral outgrowth assay performed as follows: after XX
561 days of latency reversal, supernatants of infected macrophages were incubated with CD4⁺ T-cell
562 lymphoblasts from healthy donors produced as described⁶⁵ for 7 days in RPMI 1640 with 10% FCS
563 supplemented with 10 U/ml IL-2 (Sigma-Aldrich). Lymphoblasts were centrifuged at 300g, 10 min, and
564 resuspended in fresh complete medium containing 10 U/ml IL-2 for additional 7 days. Then, lymphoblasts
565 were centrifuged again and cell pellets were processed for RT-qPCR of HIV-1 long terminal repeat as
566 described⁶⁴.

567

568 **Multiparametric Flow cytometry.** Multiparametric flow cytometry was performed as described¹² with
569 simplifications in the gating strategy: our previous experience with urethral tissues¹² allowed us to identify
570 dead cells in FSC/SSC dot plots of tissue cells suspension, gating viable cells (Supplementary Figure 3a-b).
571 Doublets were excluded in an FSC-A/FSC-H dot plot and macrophages were gated in a CD3/CD68 dot plot
572 as CD68⁺CD3^{neg} cell population (Supplementary Figure 3b-c). The antibodies used in this study were
573 designed and validated for flow cytometry and are disclosure in Supplementary Table Data 1.
574 Immunofluorescence of labeled tissue cell suspensions was acquired on an LSR II cytometer (BD
575 Biosciences). Fluorescence specificity and compensation were established in the BD CellQuest (BD
576 Biosciences) data acquisition software using BD CompBead Compensation Particles (BD Biosciences) for
577 each fluorescence-coupled antibody used in the panel.

578 Flow cytometry data were analyzed with FlowJo software (FlowJo version X 10.0.7r2 - FlowJo,
579 LCC). UMAPs were generated by concatenation of CD68⁺ cell population of 4 cART-treated HIV-infected
580 individuals followed by FlowJo UMAP plugin (S100A8, MMP7, CD206, CD163, IL-1R and IL-4R markers
581 used). Clustering analysis on UMAP was performed by FlowSom plugin to define the different macrophage
582 populations.

583 The correlation between expression of different markers comparing macrophages from different
584 origins (derived *in vitro* or obtained from urethral tissues) was performed by ClustVis software ⁶⁶ using the
585 mean percentage of macrophages expressing these markers in a total population of macrophages. The
586 correlation analysis is shown as a heatmap generated using the following parameters: correlation as
587 clustering distance and average as method for clustering between different macrophage samples; tree
588 ordering set as tightest cluster first.

589

590 ***Fluorescence in situ hybridization coupled to flow cytometry (FISH-flow)***. The detection of HIV-infected
591 cells in the tissue cell suspensions was performed by immunostaining of viral protein p24-Gag (anti-p24
592 clone KC57, FITC), combined with fluorescence *in situ* hybridization using mRNA Cy5-tagged probes
593 covering *gag*, *pol* and *env* HIV genes, both labeling being quantified at the single-cell level by flow
594 cytometry, a technique described as FISH-flow ⁶⁷. Probes were designed by Stellaris Probe Designer
595 program (<http://www.singlemoleculefish.com>) as we described ³⁴ and the probe sets are detailed in
596 Supplementary Table Data 1. FISH-flow recently succeeded in detecting the very low amount of latent HIV-
597 1 reservoir cells in cART-treated patients, which comprises around 1 infected cell per million CD4⁺ T-cells
598 ^{35, 67, 68}. The technique was performed here as described ⁶⁴ and was employed in the context of
599 multiparametric flow cytometry using a similar gating strategy as described above (Supplementary Figure
600 4c).

601

602 ***Quantification of PF4 expression in tissues***. Paraformaldehyde-fixed, paraffin-embedded urethral tissue
603 pieces were sectioned (4µm), deparaffinized in xylene and graded alcohol solutions, treated with Hydrogen
604 Peroxide solution (Advanced Cell Diagnostics, Inc.) for 10 min, heated in boiling RNAscope target retrieval
605 buffer (Advanced Cell Diagnostics, Inc.) for 30 min as recommended by manufacturer for antigen retrieval,
606 incubated with RNAscope Protease Plus (Advanced Cell Diagnostics, Inc.) for 20 min at 40°C, and washed
607 in distilled water. Sections were then blocked for nonspecific staining in a blocking solution (1% w/v BSA,
608 1% v/v horse serum, 5% v/v human serum, 1% g/v gelatin, and 50 mM EDTA) for 1h at room temperature.
609 Next, sections were labelled with 10 µg/mL CXCL4/PF4 (Chromatec, a-PF4-h1, IgG2b) and 20 µg/mL
610 CD68 (Novus, NB100-683, IgG1) antibody overnight at 4°C. After washing in blocking solution, sections
611 were incubated with 1:200 v/v Cy3-conjugated-anti-mouse-IgG2b (Jackson ImmunoResearch, 115-165-
612 207) and 1:200 v/v Cy5-conjugated-IgG1 (Abcam, ab136127) secondary antibodies for 2h at room
613 temperature. Finally, sections were washed, counterstained with DAPI and mounted with mounting medium
614 (ibidi, 50001). Immunofluorescence was visualised using a Spinning disk unit (Ixplore, Olympus) and
615 analysed using FUJI-image J software ⁶⁹. Three scans were taken from each section at ×30 magnification.
616 CXCL4/PF4 positive pixels and area per unit area were calculated as described ⁷⁰.

617

618 ***Morphological analyses of VCCs***. Confocal microscopy after immunostaining was performed as described
619 ^{6, 12} using anti-CD68 (R&D systems, 10 µg/ml) and anti-p24-Gag antibodies (EVA365 and EVA366, 1:10

620 v/v each, NIBSC, Center for AIDS Reagents). Acquired z-stacks were reconstructed into three-dimensional
621 image projections in Imaris software (version 9.0.2, Oxford Instruments plc, UK) and visualized using MIP
622 filters. Imaris creates isosurface objects by filtering and segmenting the original data set, attributing
623 dimensional data to these isosurfaces such as volume (μm^3)⁷¹. The attribution of isosurface objects based on
624 p24-Gag immunostaining in infected macrophages allowed for retrieving volumetric measures of the cluster
625 of p24-Gag signal displayed by these infected cells, corresponding to virus-containing compartments, or
626 VCC^{12, 16}. The sum of the volumes measured by all VCCs detected in one cell represents the VCC volume
627 per cell referred in this study, as described⁷².

628

629 **Morphological analyses following in situ hybridization.** Urethral macrophages were cultivated *ex vivo* in 8-
630 well detachable chamber glass slides (ThermoFisher Scientific) for HIV RNA *in situ* hybridization as
631 described^{6, 73}, using the RNAscope Multiplex Fluorescent V2 Assay kit (Advanced Cell Diagnostics, Inc.)
632 following manufacturer instructions including treating samples with 30 minutes of boiling Target Retrieval
633 Reagent and 10 minutes at 40°C of Protease Plus before hybridization and amplification steps of the
634 protocol.

635 For combined detection of HIV RNA and p24-Gag immunostaining, after *in situ* hybridization
636 procedures, samples were treated for 1 hour with a blocking buffer containing 50 mM EDTA, 0.45% cold
637 water fish gelatin (Sigma-Aldrich), 10 mg/ml BSA fraction V (Sigma-Aldrich), 1:100 v/v horse serum and
638 1:20 v/v human serum in water. Next, samples were incubated overnight at 4°C with 1:1000 v/v of anti-
639 HIV-1 p24-Gag monoclonal antibody (NIH AIDS Reagent Program, catalog number 6457) diluted in
640 blocking buffer. Samples were then incubated with anti-mouse IgG1 secondary antibody coupled to
641 AlexaFluor 488 1:2000 v/v diluted in blocking buffer, washed in PBS and incubated with 10 μM 4',6-
642 Diamidine-2'-phenylindole dihydrochloride (DAPI) for 15 minutes before coverslips were mounted on
643 slides with anti-fading medium suitable for confocal laser scanning microscopy.

644 The same protocol was applied to FISH and immunostaining of CD68 and S100A8, using for
645 detection of these markers the following primary and secondary antibodies: anti-human CD68 (R&D
646 MAB20401) and anti-human S100A8/S100A9 heterodimer (R&D MAB45701) both at 10 $\mu\text{g}/\text{ml}$, and anti-
647 mouse IgG2b coupled to AlexaFluor 488 (Jackson 115-545-207) or anti-rabbit IgG coupled to Cy5 (Jackson
648 711-177-003) both at 1:200 v/v.

649 The complete list of antibodies used in this study is found in Supplementary Table Data 2.

650

651 **Evaluation of macrophage glycolytic metabolism.** Extracellular acidification rate (ECAR) and oxygen
652 consumption rate (OCR) were measured using the XFe96 Analyzer (Agilent Technologies) as described by
653 the manufacturer.

654 To compare the metabolism of M4- and M2-macrophages, macrophages were preincubated with
655 Seahorse XF DMEM medium pH 7.4 (Agilent) supplemented with 2 mM glutamine (Glucose-free Seahorse
656 medium). The instrument was programmed to sequentially inject compounds into wells of the Seahorse

657 culture plates in the following order: Glucose (11 mM final well concentration), etomoxir (Sigma-Aldrich)
658 (100 μ M final well concentration), 2-deoxyglucose (2-DG) (Sigma-Aldrich) (10mM final well
659 concentration) and electron transport chain inhibitors antimycin A and rotenone (AM/rot)(Agilent) (10
660 μ g/ml each final well concentration). Compounds were diluted in Glucose-free Seahorse medium.

661 To compare changes in M4-macrophage metabolism upon S100A8 or LPS treatment, macrophages
662 were preincubated with Seahorse XF DMEM medium pH 7.4 (Agilent) supplemented with 2 mM glutamine
663 and 11 mM glucose (complete Seahorse medium). The instrument was programmed to sequentially inject:
664 first, the Seahorse medium alone, LPS (1 μ g/ml final well concentration) or S100A8 (10 μ g/ml final well
665 concentration) in Seahorse medium; second, etomoxir (100 μ M final well concentration); third 2-DG (10
666 mM final well concentration) and fourth, AM/rot (each 10 μ g/ml final well concentration). Compounds
667 were diluted in complete Seahorse medium.

668 Data obtained was first analyzed by Agilent Seahorse Wave Desktop software (Agilent
669 Technologies) and normalized to cells numbers per well (quantified by microscopic automatic counting
670 algorithms using Imaris software and DAPI fluorescent staining) and to baseline ECAR/OCR levels (last
671 measure before first injection). ECAR/OCR data is therefore shown as mean percentage after baseline
672 normalization (baseline levels defined as 100%). The glycolytic activity refers to a subtraction of the ECAR
673 peak level after first injection and the minimum ECAR level after 2-DG injection.

674 Energy maps were generated by plotting these ECAR peak levels against corresponding OCR
675 measures acquired at the same time point. ECAR/OCR baseline levels (last measure before first injection)
676 were normalized to correspond to 100. Arrows indicate the increase in either ECAR or OCR levels between
677 baseline measures (before first injection) and the ECAR peak (after first injection).

678
679 **Cytokines/Chemokine quantification.** Urethral mucosa tissues were processed as described ⁷⁴ to
680 obtain tissue lysates. The cytokines/chemokines CXCL4/PF4, IL-13, M-CSF, MCP-1/CCL2, TRAIL,
681 RANTES/CCL5, MIP-1 α /CCL3, GM-CSF, IL-4, MIP-3 α /CCL20 and MCP-4/CCL13 were quantified
682 using the Luminex technology (LXSAHM, R&D) on a Bio-Plex 200 (Bio-Rad) according to the
683 manufacturer's recommendations. IFN- γ was quantified using the Human IFN- γ ELISA Development Kit
684 (Mabtech), according to the manufacturer's instructions. The lower limit of quantification (LLOQ) of each
685 cytokine/chemokine is 2 pg/ml (CCL13/MCP-4 and IFN γ), 3 pg/ml (CCL20/MIP-3 α), 4 pg/ml (GM-CSF),
686 7 pg/ml (CCL5/RANTES), 10 pg/ml (TRAIL and CCL2/MCP-1), 16 pg/ml (IL-4), 100 pg/ml (CXCL4/PF4
687 and CCL3/MIP-1a) and 140 pg/ml (IL-13 and M-CSF). Correlograms were generated in R using *cor*,
688 *cor_test_mat* and *corrplot* functions.

689 S100A8/S100A8 heterodimer was measured by Quantikine ELISA kit (DS8900, R&D) according to
690 the manufacturer's recommendations.

691 Cytokine levels were normalized by the protein amount in tissue lysates (mg/ml), quantified by
692 NanoDrop spectrophotometer (ThermoFisher Scientific) using the program Protein A280.

693

694 All data associated with this study are in the paper or supplementary materials. Source data are
695 provided with this paper.

696

697 **Statistical analysis.** The results are represented as means with respective standard errors or boxplots.
698 Boxplots represent minima and maxima as lower and upper whiskers, median as centre of the box, and the
699 interquartile range Q1 and Q3 as lower and upper bounds. Statistical tests were performed by SPSS software
700 (IBM), considering normal (parametric tests, Student's *t*-test or ANOVA with post hoc pairwise
701 comparisons) or non-normal distributions (non-parametric tests, Mann-Whitney or Kruskal–Wallis), and
702 two-sided tests. Significant differences were indicated by asterisks considering *p* values below 0.05. For
703 cytokine correlograms, *cor_test_mat* function was employed with Benjamini & Hochberg (BH) adjustment.

704

705 **Data availability**

706 All data associated with this study are in the paper or supplementary materials. Source data are
707 provided with this paper.

708

709

710 **References**

711

- 712 1. Honeycutt JB, *et al.* HIV persistence in tissue macrophages of humanized myeloid-only mice during antiretroviral
713 therapy. *Nat Med* **23**, 638-643 (2017).
- 714 2. Stevenson M. Role of myeloid cells in HIV-1-host interplay. *J Neurovirol* **21**, 242-248 (2015).
- 715 3. Cassol E, Cassetta L, Rizzi C, Alfano M, Poli G. M1 and M2a polarization of human monocyte-derived
716 macrophages inhibits HIV-1 replication by distinct mechanisms. *J Immunol* **182**, 6237-6246 (2009).
- 717 4. Carter CA, Ehrlich LS. Cell biology of HIV-1 infection of macrophages. *Annu Rev Microbiol* **62**, 425-443 (2008).
- 718 5. Swingler S, Mann AM, Zhou J, Swingler C, Stevenson M. Apoptotic killing of HIV-1-infected macrophages is
719 subverted by the viral envelope glycoprotein. *PLoS Pathog* **3**, 1281-1290 (2007).
- 720 6. Real F, Sennepin A, Ganor Y, Schmitt A, Bomsel M. Live Imaging of HIV-1 Transfer across T Cell Virological
721 Synapse to Epithelial Cells that Promotes Stromal Macrophage Infection. *Cell Rep* **23**, 1794-1805 (2018).
- 722 7. Eisele E, Siliciano RF. Redefining the viral reservoirs that prevent HIV-1 eradication. *Immunity* **37**, 377-388
723 (2012).
- 724 8. Poltorak A, *et al.* Defective LPS signaling in C3H/HeJ and C57BL/10ScCr mice: mutations in Tlr4 gene. *Science*
725 **282**, 2085-2088 (1998).
- 726 9. Liou LY, Herrmann CH, Rice AP. Transient induction of cyclin T1 during human macrophage differentiation
727 regulates human immunodeficiency virus type 1 Tat transactivation function. *J Virol* **76**, 10579-10587 (2002).
- 728 10. Marchant D, Neil SJD, McKnight Á. Human immunodeficiency virus types 1 and 2 have different replication
729 kinetics in human primary macrophage culture. *Journal of General Virology* **87**, 411-418 (2006).
- 730
- 731
- 732
- 733
- 734
- 735
- 736
- 737
- 738
- 739

- 740 11. Pomerantz RJ, Feinberg MB, Trono D, Baltimore D. Lipopolysaccharide is a potent monocyte/macrophage-
741 specific stimulator of human immunodeficiency virus type 1 expression. *J Exp Med* **172**, 253-261 (1990).
742
- 743 12. Ganor Y, *et al.* HIV-1 reservoirs in urethral macrophages of patients under suppressive antiretroviral therapy. *Nat*
744 *Microbiol* **4**, 633-644 (2019).
745
- 746 13. Kruize Z, Kootstra NA. The Role of Macrophages in HIV-1 Persistence and Pathogenesis. *Front Microbiol* **10**,
747 2828 (2019).
748
- 749 14. Wong ME, Jaworowski A, Hearps AC. The HIV Reservoir in Monocytes and Macrophages. *Front Immunol* **10**,
750 1435 (2019).
751
- 752 15. Graziano F, *et al.* Extracellular ATP induces the rapid release of HIV-1 from virus containing compartments of
753 human macrophages. *Proc Natl Acad Sci U S A* **112**, E3265-3273 (2015).
754
- 755 16. Rodrigues V, Ruffin N, San-Roman M, Benaroch P. Myeloid Cell Interaction with HIV: A Complex Relationship.
756 *Front Immunol* **8**, 1698 (2017).
757
- 758 17. Ganor Y, *et al.* The adult penile urethra is a novel entry site for HIV-1 that preferentially targets resident urethral
759 macrophages. *Mucosal Immunol* **6**, 776-786 (2013).
760
- 761 18. de Sousa JR, Da Costa Vasconcelos PF, Quaresma JAS. Functional aspects, phenotypic heterogeneity, and tissue
762 immune response of macrophages in infectious diseases. *Infect Drug Resist* **12**, 2589-2611 (2019).
763
- 764 19. Chistiakov DA, Bobryshev YV, Orekhov AN. Changes in transcriptome of macrophages in atherosclerosis. *J Cell*
765 *Mol Med* **19**, 1163-1173 (2015).
766
- 767 20. De Paoli F, Staels B, Chinetti-Gbaguidi G. Macrophage phenotypes and their modulation in atherosclerosis. *Circ J*
768 **78**, 1775-1781 (2014).
769
- 770 21. Domschke G, Gleissner CA. CXCL4-induced macrophages in human atherosclerosis. *Cytokine* **122**, 154141
771 (2019).
772
- 773 22. Appelberg KS, Wallet MA, Taylor JP, Cash MN, Sleasman JW, Goodenow MM. HIV-1 Infection Primes
774 Macrophages Through STAT Signaling to Promote Enhanced Inflammation and Viral Replication. *AIDS Res Hum*
775 *Retroviruses* **33**, 690-702 (2017).
776
- 777 23. Caputa G, Castoldi A, Pearce EJ. Metabolic adaptations of tissue-resident immune cells. *Nat Immunol* **20**, 793-801
778 (2019).
779
- 780 24. Castellano P, Prevedel L, Valdebenito S, Eugenin EA. HIV infection and latency induce a unique metabolic
781 signature in human macrophages. *Sci Rep* **9**, 3941 (2019).
782
- 783 25. Valle-Casuso JC, *et al.* Cellular Metabolism Is a Major Determinant of HIV-1 Reservoir Seeding in CD4(+) T
784 Cells and Offers an Opportunity to Tackle Infection. *Cell Metab* **29**, 611-626 e615 (2019).
785
- 786 26. Gleissner CA. Macrophage Phenotype Modulation by CXCL4 in Atherosclerosis. *Front Physiol* **3**, 1 (2012).
787
- 788 27. Martinez FO, Gordon S. The M1 and M2 paradigm of macrophage activation: time for reassessment. *FI000Prime*
789 *Rep* **6**, 13 (2014).
790
- 791 28. Gordon S. Alternative activation of macrophages. *Nat Rev Immunol* **3**, 23-35 (2003).
792
- 793 29. Romagnani P, *et al.* CXCR3-mediated opposite effects of CXCL10 and CXCL4 on TH1 or TH2 cytokine
794 production. *J Allergy Clin Immunol* **116**, 1372-1379 (2005).
795
- 796 30. Gleissner CA, Shaked I, Little KM, Ley K. CXC chemokine ligand 4 induces a unique transcriptome in monocyte-
797 derived macrophages. *J Immunol* **184**, 4810-4818 (2010).
798
799

- 799 31. Scheuerer B, *et al.* The CXC-chemokine platelet factor 4 promotes monocyte survival and induces monocyte
800 differentiation into macrophages. *Blood* **95**, 1158-1166 (2000).
801
- 802 32. Domschke G, Gleissner CA. CXCL4-induced macrophages in human atherosclerosis. *Cytokine*, (2017).
803
- 804 33. Erbel C, *et al.* CXCL4-induced plaque macrophages can be specifically identified by co-expression of
805 MMP7+S100A8+ in vitro and in vivo. *Innate Immun* **21**, 255-265 (2015).
806
- 807 34. Arrigucci R, *et al.* FISH-Flow, a protocol for the concurrent detection of mRNA and protein in single cells using
808 fluorescence in situ hybridization and flow cytometry. *Nat Protoc* **12**, 1245-1260 (2017).
809
- 810 35. Baxter AE, *et al.* Single-Cell Characterization of Viral Translation-Competent Reservoirs in HIV-Infected
811 Individuals. *Cell Host Microbe* **20**, 368-380 (2016).
812
- 813 36. Butera ST. Evaluation of Compounds That Prevent Reactivation of HIV-1 in OM-10.1 Cells. *Methods Mol Med*
814 **24**, 201-206 (2000).
815
- 816 37. Vogl T, *et al.* Autoinhibitory regulation of S100A8/S100A9 alarmin activity locally restricts sterile inflammation.
817 *J Clin Invest*, (2018).
818
- 819 38. Vogl T, *et al.* Mrp8 and Mrp14 are endogenous activators of Toll-like receptor 4, promoting lethal, endotoxin-
820 induced shock. *Nat Med* **13**, 1042-1049 (2007).
821
- 822 39. Ryckman C, Robichaud GA, Roy J, Cantin R, Tremblay MJ, Tessier PA. HIV-1 transcription and virus production
823 are both accentuated by the proinflammatory myeloid-related proteins in human CD4+ T lymphocytes. *J Immunol*
824 **169**, 3307-3313 (2002).
825
- 826 40. Campillo-Gimenez L, *et al.* Neutrophils in antiretroviral therapy-controlled HIV demonstrate hyperactivation
827 associated with a specific IL-17/IL-22 environment. *J Allergy Clin Immunol* **134**, 1142-1152 e1145 (2014).
828
- 829 41. Pandiyan P, *et al.* Mucosal Regulatory T Cells and T Helper 17 Cells in HIV-Associated Immune Activation.
830 *Front Immunol* **7**, 228 (2016).
831
- 832 42. Galvan-Pena S, O'Neill LA. Metabolic reprogramming in macrophage polarization. *Front Immunol* **5**, 420 (2014).
833
- 834 43. Bouillaud F, Hammad N, Schwartz L. Warburg Effect, Glutamine, Succinate, Alanine, When Oxygen Matters.
835 *Biology (Basel)* **10**, (2021).
836
- 837 44. Bories GFP, Leitinger N. Macrophage metabolism in atherosclerosis. *FEBS Lett* **591**, 3042-3060 (2017).
838
- 839 45. French MA, King MS, Tschampa JM, da Silva BA, Landay AL. Serum immune activation markers are persistently
840 increased in patients with HIV infection after 6 years of antiretroviral therapy despite suppression of viral
841 replication and reconstitution of CD4+ T cells. *J Infect Dis* **200**, 1212-1215 (2009).
842
- 843 46. Hattab S, *et al.* Soluble biomarkers of immune activation and inflammation in HIV infection: impact of 2 years of
844 effective first-line combination antiretroviral therapy. *HIV Med* **16**, 553-562 (2015).
845
- 846 47. Sieweke MH, Allen JE. Beyond stem cells: self-renewal of differentiated macrophages. *Science* **342**, 1242974
847 (2013).
848
- 849 48. Deeks SG, Tracy R, Douek DC. Systemic effects of inflammation on health during chronic HIV infection.
850 *Immunity* **39**, 633-645 (2013).
851
- 852 49. Churchill MJ, Deeks SG, Margolis DM, Siliciano RF, Swanstrom R. HIV reservoirs: what, where and how to
853 target them. *Nat Rev Microbiol* **14**, 55-60 (2016).
854
- 855 50. Perkins DJ, Patel MC, Blanco JC, Vogel SN. Epigenetic Mechanisms Governing Innate Inflammatory Responses.
856 *J Interferon Cytokine Res* **36**, 454-461 (2016).
857
- 858 51. Nathan C, Ding A. Nonresolving inflammation. *Cell* **140**, 871-882 (2010).

- 859
860 52. Foell D, Wittkowski H, Vogl T, Roth J. S100 proteins expressed in phagocytes: a novel group of damage-
861 associated molecular pattern molecules. *J Leukoc Biol* **81**, 28-37 (2007).
862
863 53. Kawai T, Akira S. Signaling to NF-kappaB by Toll-like receptors. *Trends Mol Med* **13**, 460-469 (2007).
864
865 54. Hashemi FB, *et al.* Myeloid-related protein (MRP)-8 from cervico-vaginal secretions activates HIV replication.
866 *AIDS* **15**, 441-449 (2001).
867
868 55. Endoh Y, Chung YM, Clark IA, Geczy CL, Hsu K. IL-10-dependent S100A8 gene induction in
869 monocytes/macrophages by double-stranded RNA. *J Immunol* **182**, 2258-2268 (2009).
870
871 56. Strasser F, Gowland PL, Ruef C. Elevated serum macrophage inhibitory factor-related protein (MRP) 8/14 levels
872 in advanced HIV infection and during disease exacerbation. *J Acquir Immune Defic Syndr Hum Retrovirol* **16**, 230-
873 238 (1997).
874
875 57. Cohn LB, Chomont N, Deeks SG. The Biology of the HIV-1 Latent Reservoir and Implications for Cure
876 Strategies. *Cell Host Microbe* **27**, 519-530 (2020).
877
878 58. Russell DG, Huang L, VanderVen BC. Immunometabolism at the interface between macrophages and pathogens.
879 *Nat Rev Immunol* **19**, 291-304 (2019).
880
881 59. Koo SJ, Garg NJ. Metabolic programming of macrophage functions and pathogens control. *Redox Biol* **24**, 101198
882 (2019).
883
884 60. Palmer CS, Palchadhuri R, Albargy H, Abdel-Mohsen M, Crowe SM. Exploiting immune cell metabolic
885 machinery for functional HIV cure and the prevention of inflammaging. *F1000Res* **7**, 125 (2018).
886
887 61. Netea MG, *et al.* Trained immunity: A program of innate immune memory in health and disease. *Science* **352**,
888 aaf1098 (2016).
889
890 62. Clayton KL, *et al.* Resistance of HIV-infected macrophages to CD8(+) T lymphocyte-mediated killing drives
891 activation of the immune system. *Nat Immunol* **19**, 475-486 (2018).
892
893 63. Mantovani A, Sica A, Sozzani S, Allavena P, Vecchi A, Locati M. The chemokine system in diverse forms of
894 macrophage activation and polarization. *Trends Immunol* **25**, 677-686 (2004).
895
896 64. Real F, *et al.* Platelets from HIV-infected individuals on antiretroviral drug therapy with poor CD4(+) T cell
897 recovery can harbor replication-competent HIV despite viral suppression. *Sci Transl Med* **12**, (2020).
898
899 65. Siliciano JD, Siliciano RF. Enhanced culture assay for detection and quantitation of latently infected, resting CD4+
900 T-cells carrying replication-competent virus in HIV-1-infected individuals. *Methods Mol Biol* **304**, 3-15 (2005).
901
902 66. Metsalu T, Vilo J. ClustVis: a web tool for visualizing clustering of multivariate data using Principal Component
903 Analysis and heatmap. *Nucleic Acids Res* **43**, W566-570 (2015).
904
905 67. Baxter AE, *et al.* Multiparametric characterization of rare HIV-infected cells using an RNA-flow FISH technique.
906 *Nat Protoc* **12**, 2029-2049 (2017).
907
908 68. Grau-Exposito J, *et al.* A Novel Single-Cell FISH-Flow Assay Identifies Effector Memory CD4+ T cells as a
909 Major Niche for HIV-1 Transcription in HIV-Infected Patients. *MBio* **8**, (2017).
910
911 69. Schindelin J, *et al.* Fiji: an open-source platform for biological-image analysis. *Nat Methods* **9**, 676-682 (2012).
912
913 70. Yeo L, *et al.* Expression of chemokines CXCL4 and CXCL7 by synovial macrophages defines an early stage of
914 rheumatoid arthritis. *Ann Rheum Dis* **75**, 763-771 (2016).
915
916 71. Real F, Mortara RA. The diverse and dynamic nature of Leishmania parasitophorous vacuoles studied by
917 multidimensional imaging. *PLoS Negl Trop Dis* **6**, e1518 (2012).
918

- 919 72. Leymarie O, *et al.* Contribution of the Cytoplasmic Determinants of Vpu to the Expansion of Virus-Containing
 920 Compartments in HIV-1-Infected Macrophages. *J Virol* **93**, (2019).
 921
 922 73. Deleage C, *et al.* Defining HIV and SIV Reservoirs in Lymphoid Tissues. *Pathog Immun* **1**, 68-106 (2016).
 923
 924 74. Sennepin A, *et al.* The Human Penis Is a Genuine Immunological Effector Site. *Front Immunol* **8**, 1732 (2017).
 925
 926

927

928 **Acknowledgements**

929

930 The authors thank the tissue donors for their kind participation in the study. This study was
 931 supported by l’Agence Nationale de Recherches sur le Sida et les Hépatites Virales (ANRS) (AO2015-2-
 932 17046) and SIDACTION (15CONV03), and Fondation pour la Recherche Medicale (Equipe FRM:
 933 EQU201903007830) funds to MB. FR received post-doctoral fellowship from SIDACTION and ANRS, AZ
 934 is a doctoral fellow from the China Scholarship Council (CSC), and AS received a post-doctoral fellowship
 935 from ANRS.

936

937 **Author contributions statement**

938 FR, MB: conceived the experiments; MR and SC: collected the patient samples and provided
 939 clinical information; FR, AS and MB: performed and analyzed flow cytometry experiments; FR, AZ, AB,
 940 BH and MB performed and analyzed confocal microscopy after immunostaining and *in situ* hybridization;
 941 FR, AZ, MB: devised and performed viral outgrowth assays; FR, RA, MLG, MB: set up fluorescence *in situ*
 942 hybridization coupled to flow cytometry; JR and TV: provided S100 proteins and FR, JR ,TV and MB
 943 analyzed S100A8 experimental results; FR, AZ, CR, AL, FB, MB: devised, performed and analyzed
 944 Seahorse Analyzer experiments; FR, and MB: wrote the manuscript.

945

946 **Competing interested statement**

947 The authors declare no competing interests in conducting this study.

948

949 **Tables**

Individual	Age at tissue sampling	years of HIV diagnostic	years of cART initiation	viral load at sampling	cART regimen ¹
1	30	3	NA	undetectable	NA
2	50	NA	NA	undetectable	NA
3	43	22	NA	undetectable	RTV DRV RAL ETR
4	38	23	NA	undetectable	FTC TDF RTV
5	38	NA	NA	undetectable	NA

6	53	NA	11	undetectable	FTC TDF EVG
7	59	NA	NA	undetectable	FTC TDF EVG
8	51	4	NA	undetectable	3TC DTG ABC
9	34	3	3	undetectable	FTC TDF EVG
10	40	14	11	undetectable	FTC TDF EVG
11	41	NA	NA	undetectable	NA
12	36	NA	NA	undetectable	NA
13	59	13	13	undetectable	DTG RPV
14	26	9	9	undetectable	FTC TDF EFV
15	37	8	NA	undetectable	FTC TDF EFV
16	35	16	9	undetectable	FTC TDF RTV DRV
17	32	2	2	undetectable	NA
18	45	18	18	undetectable	3TC ABC LPV RTV
19	45	4	4	undetectable	FTC TDF RTV DRV
20	47	28	10	undetectable	FTC TDF RPV
21	36	10	2	undetectable	3TC DTG ABC
22	65	4	4	undetectable	NA
23	49	24	22	undetectable	3TC DTG
24	44	15	14	undetectable	FTC TDF RPV
25	51	NA	NA	undetectable	NA

¹cART includes nucleoside reverse transcriptase inhibitors (3TC, lamivudine; ABC, abacavir; FTC, emtricitabine; TDF, tenofovir), non-nucleoside reverse transcriptase inhibitors (EFV, efavirenz; ETR, etravirine; RPV, rilpivirine), protease inhibitors (ATV, atazanavir; DRV, darunavir; FPV, fosamprenavir; RTV, ritonavir; LPV, lopinavir) and integrase inhibitors (DTG, dolutegravir; EVG, elvitegravir; RAL, raltegravir). NA, not available.

950

951 **Table 1. Clinical information of HIV-infected cART-suppressed individuals enrolled in this study.** Table
952 shows the age, years after HIV positive diagnostic and years under combined antiretroviral therapy (cART) of
953 the individuals at the date of tissue sampling. The viral load of these individuals was tested undetectable at date
954 of sampling (HIV RNA copies/ml of blood below the limit of detection of 40 copies/ml). All individuals were
955 receiving different suppressive cART regimens at sampling, although not all regimens were fully disclosed (not
956 available, NA).

957

958 **Figure legends**

959

960 **Figure 1. Inflammatory M4-macrophages are enriched in the urethral mucosa of cART-suppressed HIV-1**
961 **infected-individuals.**

962 (a) Scheme of the different methods applied to evaluate morphologically and functionally the mucosal
963 macrophage HIV reservoir, from processing 0.5 x 0.5 cm mucosal tissue pieces obtained from individuals that
964 underwent gender reassignment.

965 (b) CXCL4/PF4, IL-13 and IFN- γ cytokine profile of urethral tissue extracts of healthy donors (grey) and cART-
966 suppressed HIV-infected (cART HIV⁺) individuals (red). The number of individual samples (n) included in the
967 analysis is shown per group and cytokine tested. Mann-Whitney test performed for pairwise comparisons
968 between the two groups of individuals and per cytokine. Source data provided in Source Data file.

969 (c) Flow cytometry gating strategy for characterization of M4-macrophage subtype in healthy donors (upper
970 example) and cART-suppressed HIV-infected individuals (lower example). From CD68⁺ CD3^{neg} events (total
971 M Φ), M4-macrophages are defined as S100A8⁺MMP-7⁺ events. Frequencies of total M Φ and M4-macrophages
972 among total M Φ are shown as mean with 95% confidence interval in brackets.

973 (d) Percentage of total M Φ among the tissue cell suspension (Total M Φ population) and percentage of M4-
974 macrophages among total M Φ population (M4 M Φ in total M Φ) in healthy donors (grey, n=7) and cART-
975 suppressed HIV-infected individuals (red, n=7). Mann-Whitney test between healthy donor and cART HIV⁺
976 group. Source data provided in Source Data file.

977 (e) Frequency in percentage of macrophage polarization markers displayed by total M Φ among the tissue cell
978 suspension (Total M Φ population, left graph) and M4-macrophages (M4-macrophages population, right graph)
979 in healthy donors (grey, n=7) and cART-suppressed HIV-infected individuals (red, n=7). Mann-Whitney test
980 between healthy donor and cART HIV⁺ group. Source data provided in Source Data file.

981

982 **Figure 2. HIV-1 mucosal macrophage reservoirs form in inflammatory IL-1R⁺ M4-macrophages *in vivo* as**
983 **detected at single-cell level.**

984 (a) Identification of HIV reservoir in macrophages identified by HIV RNA detection using FISH coupled to
985 CD68 immunostaining on paraffin-embedded urethral tissue sections from a cART-treated HIV-infected
986 individual. HIV RNA in red, macrophage marker CD68 in green, nuclei stained with DAPI (blue). Image shows
987 the different fluorescent channels of a macrophage HIV reservoir and a high-magnification inset on the right
988 with these channels merged. Bar=10 μ m or 3 μ m (inset). Image is representative of two cART-treated HIV-
989 infected individual samples.

990 (b) Representative flow cytometry gating of HIV RNA⁺p24-Gag⁺ events acquired in total urethral M Φ
991 population obtained from a healthy donor (upper) and a cART-suppressed HIV-infected individual (lower).
992 Frequencies of HIV RNA⁺/p24-Gag⁺ M Φ among total M Φ are shown as mean with 95% confidence interval in
993 brackets (n=5 healthy donors, n=5 cART HIV-infected individuals).

994 (c) Percentage of HIV RNA⁺p24-Gag⁺ events acquired in total urethral M Φ population obtained from these two
995 groups of individuals (n=5 healthy donors, n=5 cART HIV-infected individuals). Dotted red line indicates limit
996 of detection based on healthy donor controls. Mann-Whitney test. Source data provided in Source Data file.

997 (d) UMAP built from concatenating CD68⁺ cell populations of different cART HIV⁺ individuals (n=4) after
998 clustering analysis of macrophage populations. HIV⁺ macrophages were backgated into the UMAP to identify
999 which macrophage profile harbors HIV in cART-treated individuals.

1000 (e) S100A8 is expressed by HIV reservoir macrophages as shown by colocalization of HIV RNA detected using
1001 FISH coupled to CD68 and S100A8 immunostaining on paraffin-embedded urethral tissue sections from two
1002 cART-treated HIV-infected individuals (#1 and #2). HIV RNA in red, macrophage marker CD68 in green,
1003 S100A8 in magenta, nuclei stained with DAPI (blue). Image shows the different fluorescent channels (separated
1004 and merged) of the detected macrophage HIV reservoirs found in the mucosal stroma. A high-magnification
1005 inset for the one detected in individual #2 is shown on the right, with fluorescent channels merged. Bar=10 μm
1006 or 3 μm (inset).

1007

1008 **Figure 3. M4-MDM and tissue macrophages from healthy donors infected *in vitro/ex vivo* are surrogates**
1009 **of HIV-1 mucosal macrophage reservoirs.**

1010 (a) Hierarchical clustering heatmap of macrophage polarization markers and different macrophage subtypes
1011 (obtained *in vivo* or *in vitro*-derived by different stimuli). The intensity of the red color boxes refers to
1012 correlation z-scores. Data were obtained from four independent experiments. Source data provided in Source
1013 Data file.

1014 (b) Cumulative viral production assessed in *in vitro*-derived MΦ culture supernatants at different days after
1015 infection. M2-MDM in blue, non-polarized GM-CSF/M-CSF-derived MDM in grey and M4-MDM in red. Data
1016 refers to one experiment representative of three independent experiments. Source data provided in Source Data
1017 file.

1018 (c-d) Confocal microscope images of M4-MDM latently infected *in vitro* (34 days post-infection) (n=3) (c) and
1019 infected tissue macrophage obtained from cART-suppressed HIV-infected individuals (n=2) (d), immunolabeled
1020 for p24-Gag (green) and CD68 (red). Nuclei were stained with DAPI. Merged images are shown as xy
1021 projections (main images) and xz/yz projections (framed VCC a, VCC b and VCC c in C right insets, and in D,
1022 lower right insets). In D, VCCs framed and magnified in the upper-right inset showing p24-Gag⁺ fluorescence
1023 signal only. Bar= 1, 5, or 10 μm.

1024 (e-f) Volumetric morphometry of VCCs in infected macrophages obtained from M4-MDM latently infected *in*
1025 *vitro* (n=3) (E) or cART-suppressed HIV-infected tissues (n=2 individuals) (f) after image segmentation in VCC
1026 isosurfaces. Dot-plots show the volumes (μm³) of each VCC isosurface detected in different macrophages
1027 (identified by number #) obtained from different donors (identified by donor number #). Boxplots represent the
1028 sum of VCC volumes per macrophage. Upper panels show VCC isosurfaces (in green, 3D rendering) segmented
1029 from the confocal images of infected macrophages. Source data provided in Source Data file.

1030 (g) Cumulative viral production assessed in the supernatants of tissue macrophages obtained from healthy
1031 donors (discriminated by different colors, n=4) and infected *ex vivo* at different days after infection. Source data
1032 provided in Source Data file.

1033 (h) Cumulative viral production measured in the supernatants of *ex vivo* infected urethral macrophages (pool of
1034 three healthy donors) in the absence or presence of 10 μ M AZT. Source data provided in Source Data file.

1035

1036 **Figure 4. S100A8 reactivate the production of replication-competent virus from tissue macrophage**
1037 **reservoirs.**

1038 (a) Quantification of S100A8 monomers and S100A8/S100A9 heterodimers in urethral tissue extracts of healthy
1039 donors (grey, n=9) and cART-suppressed HIV-infected individuals (cART HIV⁺) (red, n=6). Mann-Whitney test
1040 between healthy donor and cART HIV⁺ group. Source data provided in Source Data file.

1041 (b) S100A8 cellular expression quantified by flow cytometry of urethral cell suspensions expressed as
1042 percentage of S100A8⁺ cells among the entire tissue cell population and among CD68⁺ M Φ , or as S100A8 Mean
1043 Fluorescence Intensity (MFI) in S100A8⁺ cells detected among the entire tissue cell population, among
1044 CD68⁺M Φ , or among M4 M Φ . Mann-Whitney test between healthy donor (n=5) and cART HIV⁺ group (n=7).
1045 Source data provided in Source Data file.

1046 (c) Viral production quantified in M4-MDM culture supernatants after latent infection followed by 2 days of
1047 latency reversal induced by indicated S100A8 concentrations or 1 μ g/ml LPS. Non-reactivated controls refer to
1048 untreated M4-MDM latently infected macrophages. Mann-Whitney test between non-reactivated (untreated) and
1049 treated groups pairwise. Data were obtained from five independent experiments. Source data provided in Source
1050 Data file.

1051 (d) HIV-1 latency reversal of tissue macrophages obtained from healthy donors latently infected *ex vivo* (n=3),
1052 expressed as ratio between macrophage-associated HIV-LTR RNA copies per M Φ and the peak cumulative viral
1053 production per M Φ before latency, after 2 days of S100A8 or LPS treatment. Non-reactivated controls refer to
1054 ratio from untreated latently infected tissue macrophages. Mann-Whitney test between non-reactivated
1055 (untreated) and treated groups pairwise. Source data provided in Source Data file.

1056 (e) Outgrowth of replicating virus produced by tissue macrophage reservoirs obtained from cART-suppressed
1057 HIV-infected individuals after S100A8- or LPS-induced latency reversal, expressed as HIV LTR RNA copies
1058 per million CD4⁺ T-cell lymphoblasts from the outgrowth assays. Non-reactivated controls refer to untreated
1059 tissue macrophage reservoirs. Pairwise Mann-Whitney test between non-reactivated (untreated, n=5) and treated
1060 groups (S100A8, n=5; LPS, n=4). Source data provided in Source Data file.

1061

1062

1063 **Figure 5. S100A8-mediated reactivation of HIV macrophage reservoirs depends on a glycolytic metabolic**
1064 **shift.**

1065 (a) Extracellular Acidification (ECAR) and Oxygen Consumption Rate (OCR) of M2-MDM (grey) or M4-MDM
1066 (red) cultures measured after sequential addition of Seahorse medium with glucose, etomoxir (eto), 2-
1067 deoxyglucose (2-DG) and antimycin/rotenone (AM/rot). Results are shown as mean percentages (+/- SEM) of

1068 rate increase/decrease from baseline rate (time point before glucose injection) for each technical replicate. Data
1069 obtained from n=4 independent experiments. Source data provided in Source Data file.

1070 (b) Glycolytic activity of M2-MDM (grey) or M4-MDM (red) groups, which refers to the maximum ECAR
1071 reached after glucose injection deduced from the minimum ECAR reached after 2-DG injection. Mann-Whitney
1072 test. Data obtained from n=4 independent experiments. Source data provided in Source Data file.

1073 (c) ECAR and OCR measured in M4-MDM cultures non-stimulated (medium with glucose) or stimulated with
1074 S100A8 or LPS in the presence of glucose, followed by sequential injection of etomoxir (eto), 2-deoxyglucose
1075 (2-DG) and antimycin/rotenone (AM/rot). Results are displayed as mean percentages (+/- SEM) of rate
1076 increase/decrease from baseline rate (time point before glucose injection) for each technical replicate. Data
1077 obtained from n=4 independent experiments. Source data provided in Source Data file.

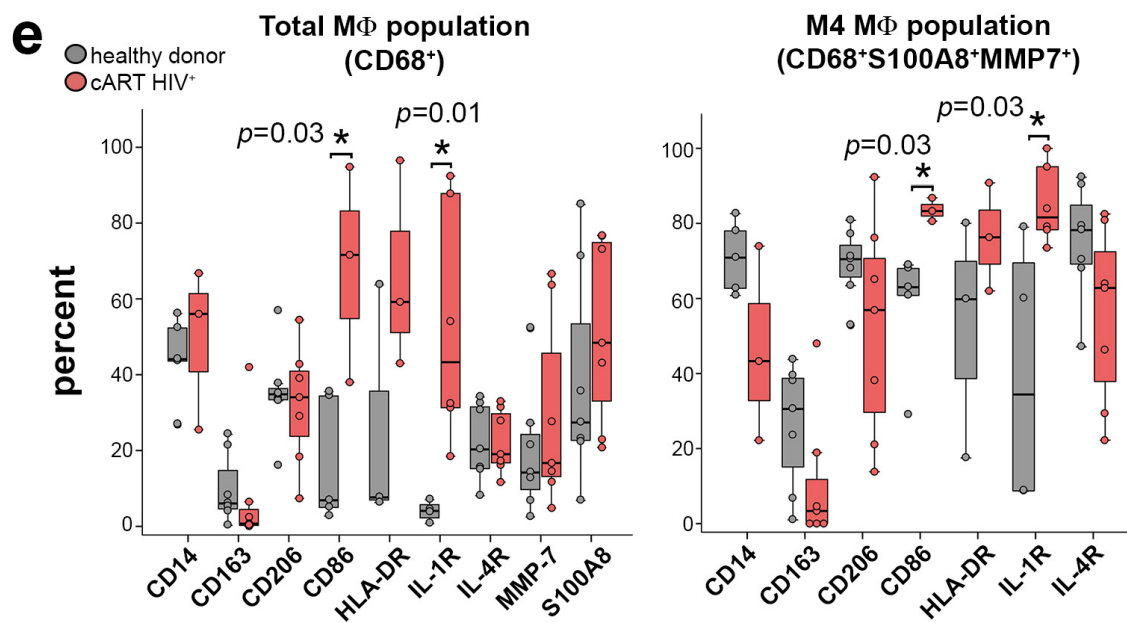
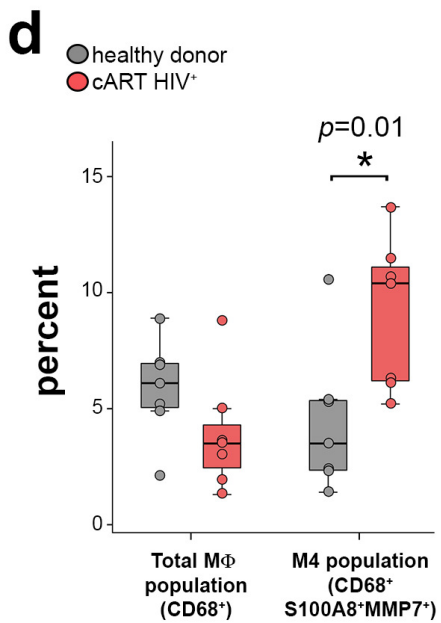
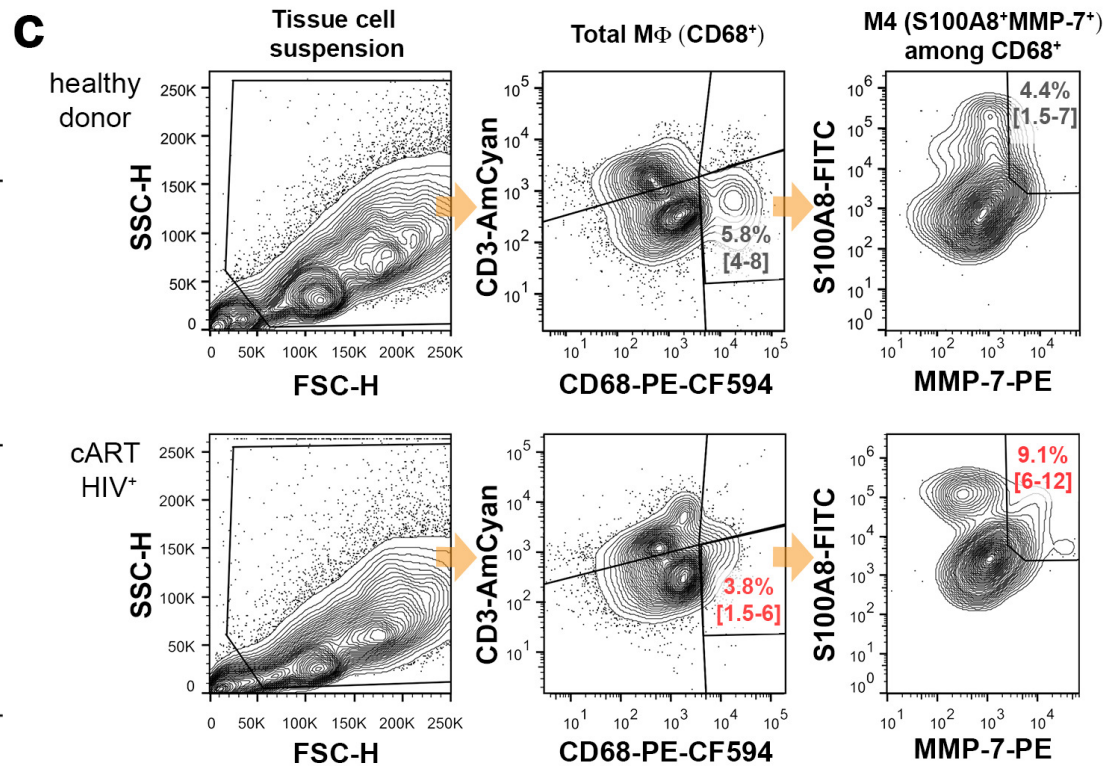
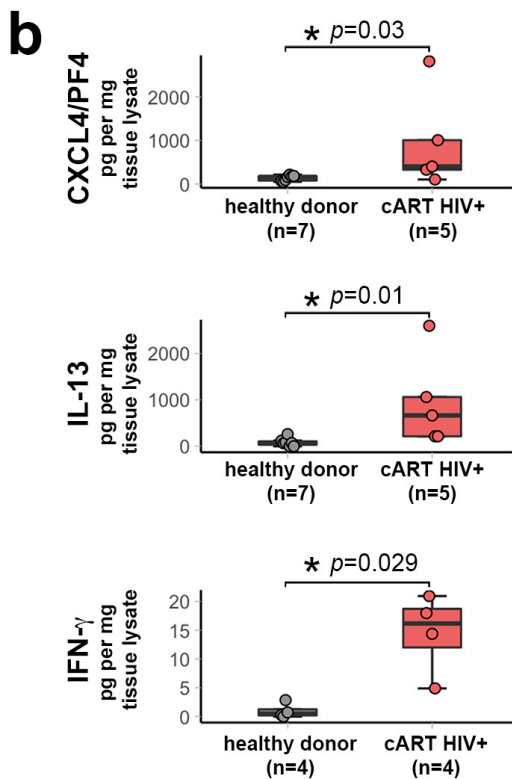
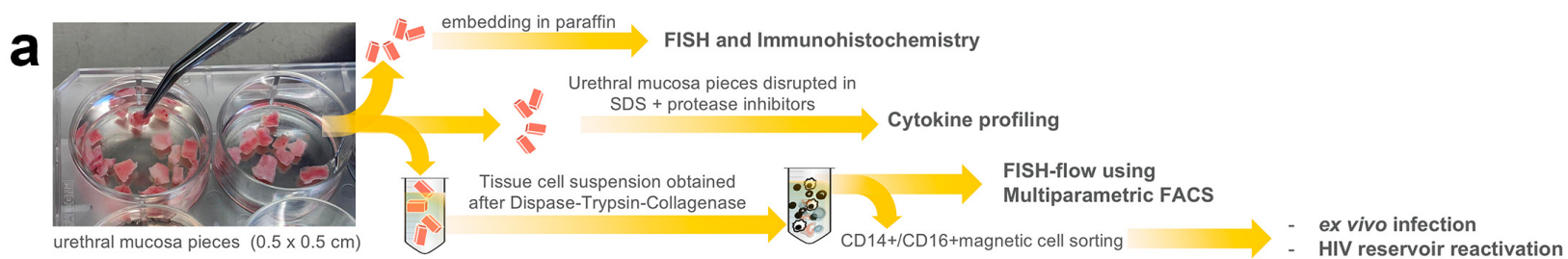
1078 (d) Glycolytic activity of non-stimulated and S100A8- or LPS-stimulated M4-MDM. ANOVA with Bonferroni
1079 post hoc test. Data obtained from n=4 independent experiments. Source data provided in Source Data file.

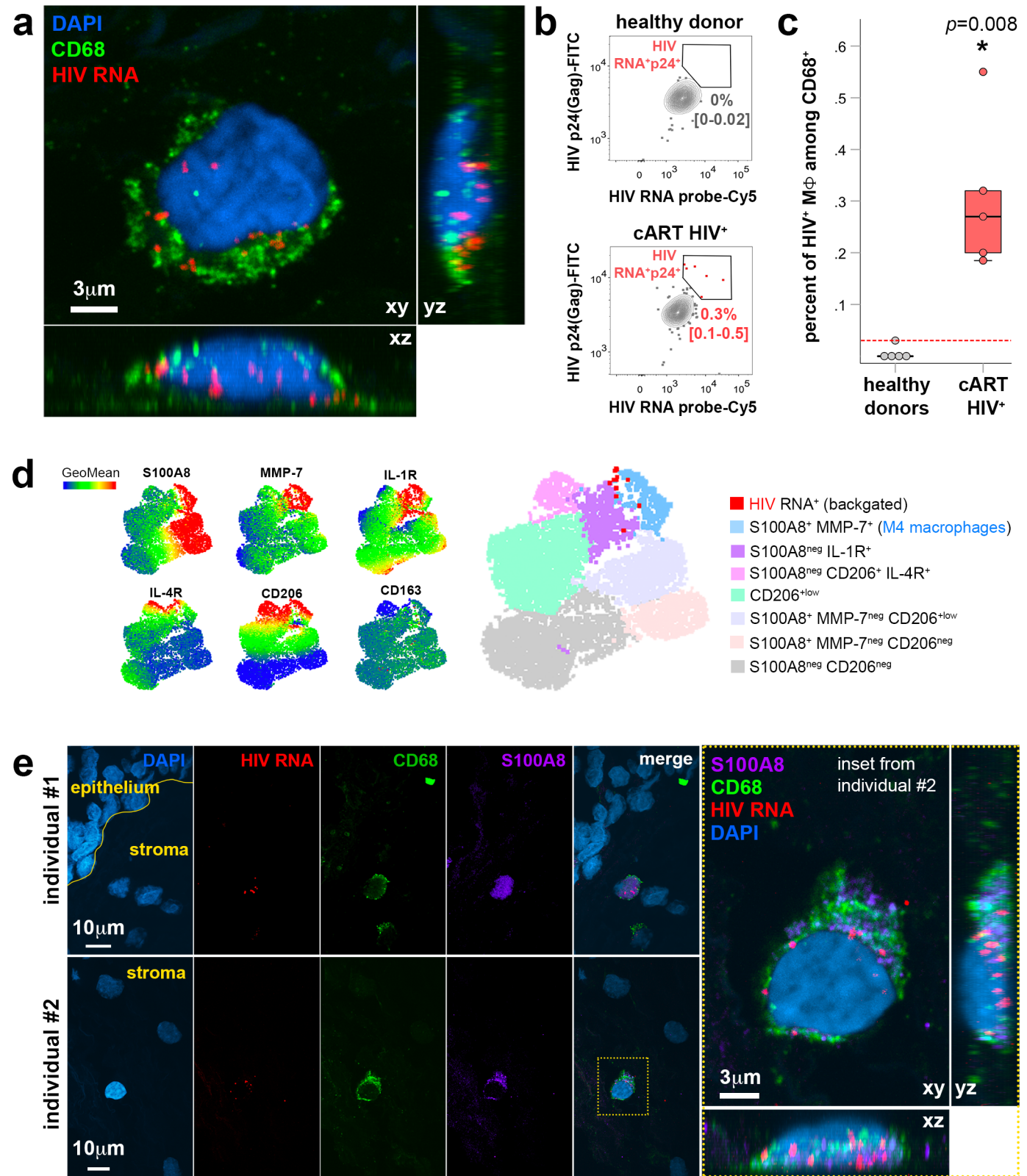
1080 (e-f) Outgrowth of replicating virus produced by tissue macrophage reservoirs obtained from cART-suppressed
1081 HIV-infected individuals after S100A8 latency reversal with or without 2-DG pre-treatment. (e) Scheme of the
1082 experiment measuring the reactivation of macrophage HIV reservoirs obtained *in vivo* from urethral tissues *ex*
1083 *vivo* using the different stimuli, namely S100A8, S100A8 preceded by a 2-DG pre-treatment, and LPS. The
1084 supernatants of reactivated macrophages were added to CD4⁺T-cells in an outgrowth assay which readout is the
1085 detection of HIV RNA in the CD4⁺T-cells by qPCR. (f) Outgrowth of virus produced by reactivated macrophage
1086 HIV reservoirs expressed as cell-associated HIV LTR RNA copies per million CD4⁺ T-cell lymphoblasts
1087 employed in outgrowth assays. Non-reactivated controls refer to untreated tissue macrophage reservoirs.
1088 ANOVA with Bonferroni correction. Data were obtained from three different cART HIV-infected individuals.
1089 Source data provided in Source Data file.

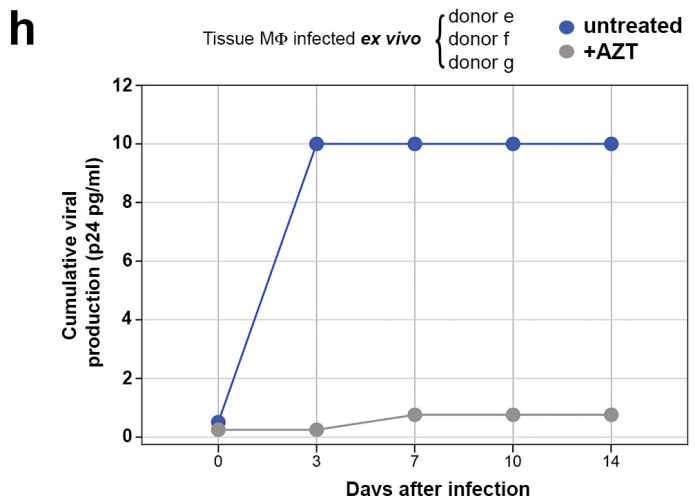
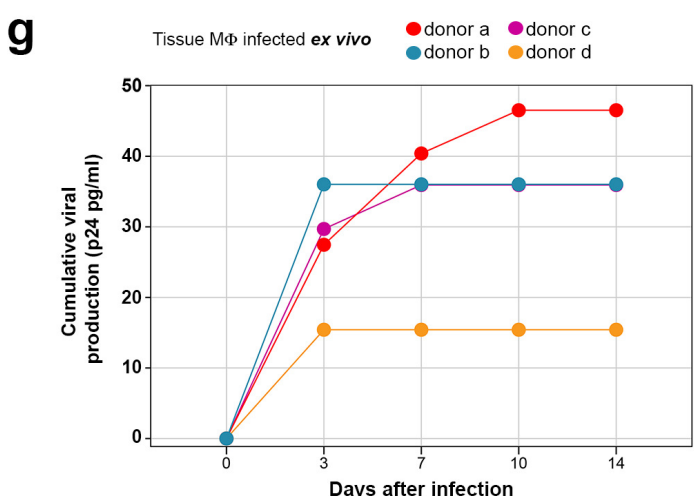
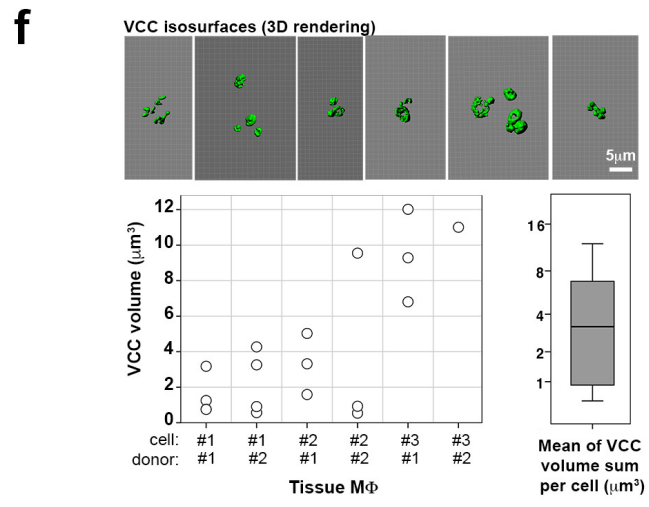
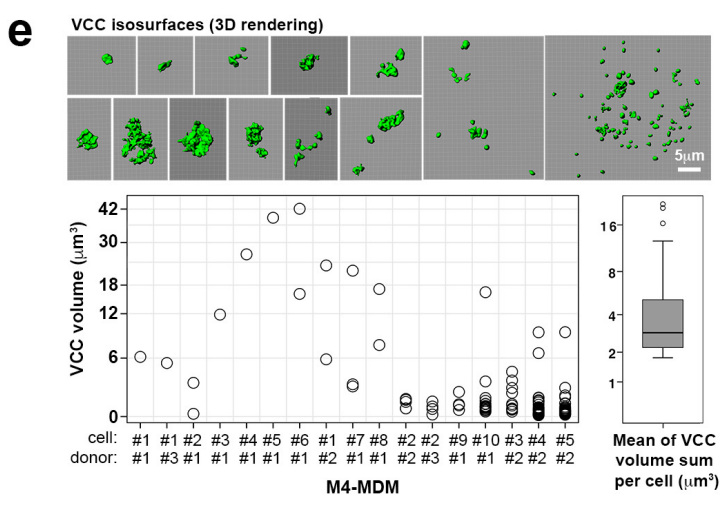
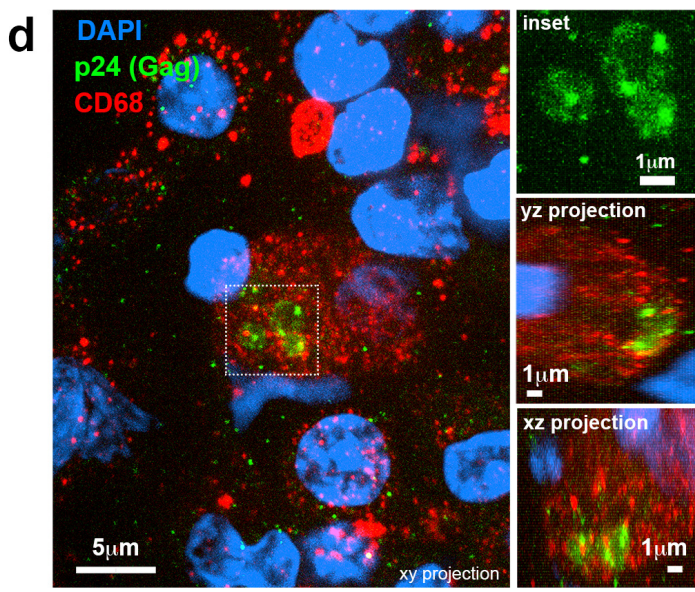
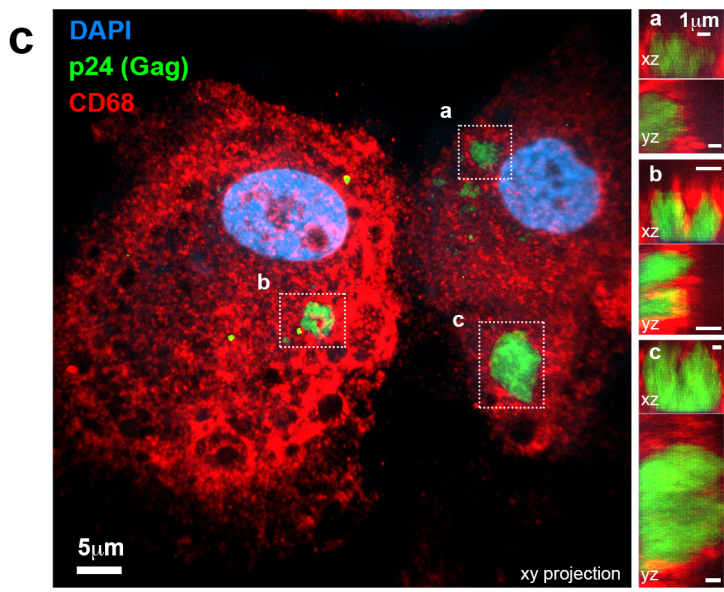
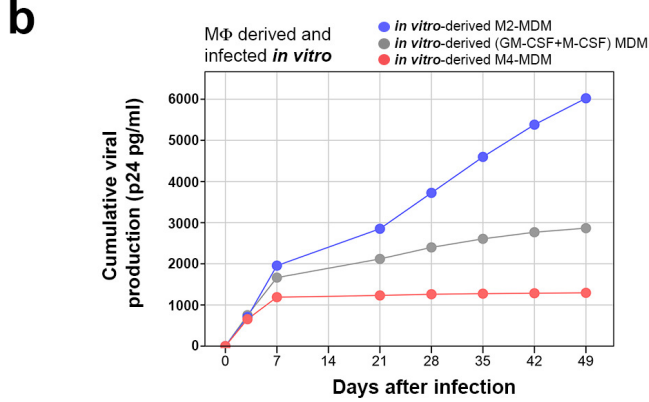
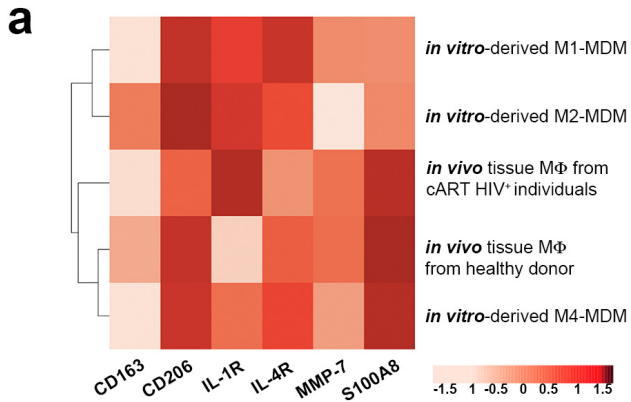
1090

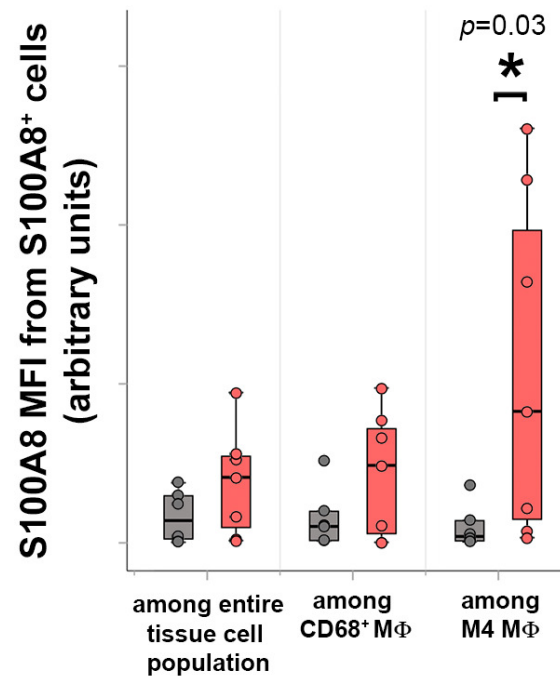
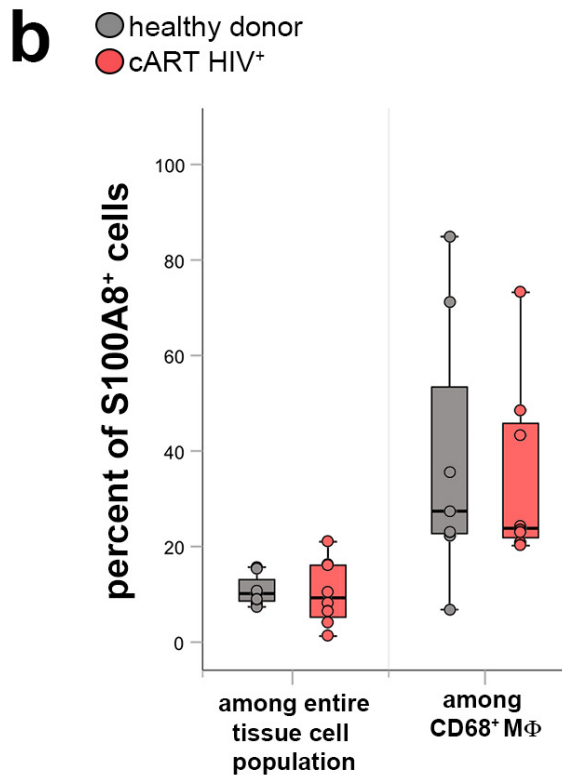
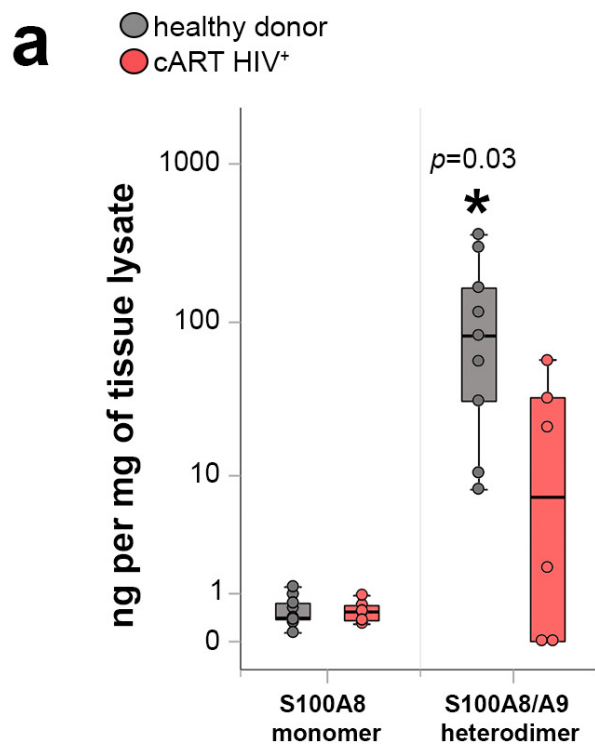
1091

1092

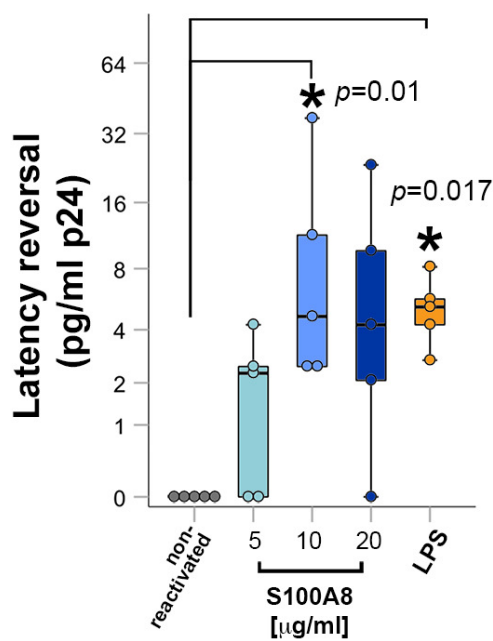




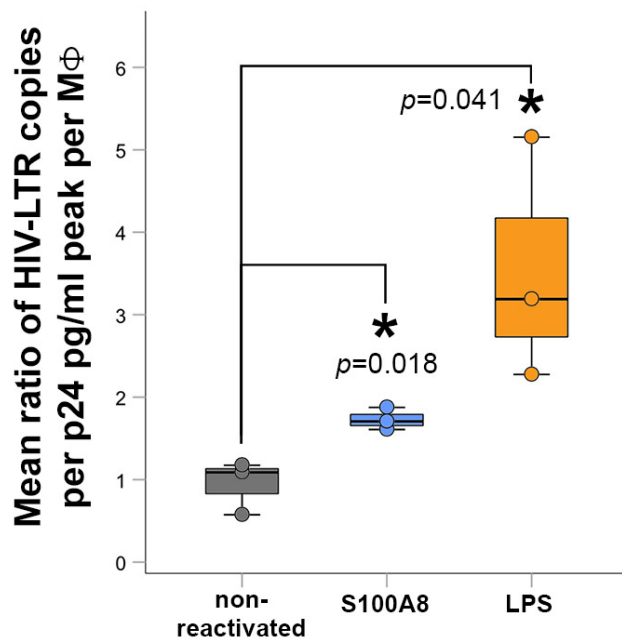




c M4-MDM latently infected and reactivated *in vitro*



d Tissue MΦ latently infected and reactivated *in vitro*



e Tissue MΦ from cART HIV⁺ individuals, reactivated *ex vivo*

